NASA TECHNICAL REPORT

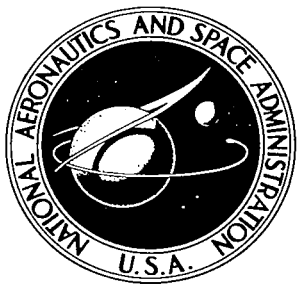


NASA TR R-202

LOAN COPY: I
AFWL (W
KIRTLAND AF
0067983
TECH LIBRARY KAFB, NM

NASA TR R-202

# THEORETICAL AERODYNAMIC CHARACTERISTICS OF SHARP AND CIRCULARLY BLUNT-WEDGE AIRFOILS

*by Joseph W. Cleary and John A. Axelson*

*Ames Research Center*

*Moffett Field, Calif.*

NATIONAL AERONAUTICS AND SPACE ADMINISTRATION • WASHINGTON, D. C. • JULY 1964

TECH LIBRARY KAFB, NM

0067913

# THEORETICAL AERODYNAMIC CHARACTERISTICS OF SHARP AND CIRCULARLY BLUNT-WEDGE AIRFOILS

By Joseph W. Cleary and John A. Axelson

Ames Research Center
Moffett Field, Calif.

NATIONAL AERONAUTICS AND SPACE ADMINISTRATION

For sale by the Office of Technical Services, Department of Commerce,
Washington, D.C. 20230 -- Price $1.00

# THEORETICAL AERODYNAMIC CHARACTERISTICS OF SHARP AND CIRCULARLY BLUNT-WEDGE AIRFOILS AT HYPERSONIC SPEEDS

By Joseph W. Cleary and John A. Axelson

Ames Research Center
Moffett Field, Calif.

## SUMMARY

The inviscid hypersonic aerodynamic characteristics of circularly blunt-wedge airfoils are derived from numerical solutions. Hypersonic wedge theory based on explicit oblique-shock equations is shown to provide rapid estimates of the pressures over both sharp and blunt airfoils. The effects of varying the airfoil wedge angle and bluntness and of varying the gas specific-heat ratio are evaluated.

The hypersonic wedge theory provides an accurate prediction of the conditions at shock detachment for sharp airfoils for any value of gas specific-heat ratio. For the limiting case of infinite Mach number and a specific-heat ratio of unity, the theory is in agreement with Newtonian impact theory. The exact maximum lift-drag ratios and the lift coefficients at maximum lift-drag ratio for sharp airfoils at infinite Mach number are shown.

Variation of gas specific-heat ratio is shown to have large effects on the aerodynamic characteristics of blunt and sharp airfoils at hypersonic Mach numbers. The lift curves are demonstrated to be highly nonlinear and to depart significantly from impact theory as the gas specific-heat ratio is increased.

## INTRODUCTION

Both sharp and blunt airfoils are of interest for hypersonic flight. Sharp leading edges are desirable from the standpoint of reducing drag and thereby achieving efficient hypersonic airfoil performance with increased lift-to-drag ratios. Primary interest in sharp airfoils has generally been directed to the lower end of the hypersonic speed range where convective heating presents no insurmountable difficulties. Useful techniques for estimating the hypersonic aerodynamic characteristics of sharp, thin airfoils at small angles of attack were developed in references 1, 2, and 3 using hypersonic similarity laws and small-disturbance approximations. One of the significant results to arise from these earlier studies is that, within the limited scope of airfoils and angles of attack covered, the hypersonic airfoil having a flat windward surface appears to offer the optimum ratio of lift to drag. However, these earlier studies did not cover the problem of predicting airfoil characteristics at larger angles of attack up to shock

detachment. The predictions of these characteristics for sharp airfoils was undertaken in the present study and includes the assessment of the effect of variable gas specific-heat ratio.

The problems imposed by aerodynamic convective heating in the hypersonic flight range have been met with the use of bluntness on both the noses of bodies of revolution and along the leading edges of planar surfaces. Various theoretical methods are available for predicting the hypersonic characteristics of blunt airfoils. The simplest is the approximation of Newtonian impact theory which has application to three-dimensional bodies but is questioned in its applicability to planar shapes. Another more exact method, which is extensively used in the present report, is the accurate numerical blunt body and characteristics solution performed on an electronic computer. Other simpler approaches are needed for accurately estimating the hypersonic aerodynamic characteristics of both sharp and blunt airfoils. The present study was pursued with the development of such a simpler method as one of its primary objectives. For the numerical solutions, only airfoils having circularly blunt leading edges and flat aftersurfaces are considered. The selection of a circular leading edge leads to simplifications in the theoretical methods and flat aftersurfaces are consistent with the optimum properties of sharp airfoils having flat windward surfaces. Numerical solutions of sufficient scope were obtained to evaluate the effects of wedge airfoil angle and bluntness for specific-heat ratios of 1.400 and 1.667. Through the use of oblique-shock theory and simple hypersonic concepts, the numerical solutions are correlated. The solutions and correlations provide means for making rapid accurate estimates of the hypersonic aerodynamic characteristics of both blunt- and sharp-wedge airfoils.

## SYMBOLS

$C_p$ pressure coefficient, $\frac{p-p_\infty}{q_\infty}$

$c$ chord

$c_d$ section drag coefficient, $\frac{\text{drag}}{q_\infty c}$

$c_d'$ drag-coefficient component, $\frac{\text{drag component}}{q_\infty R}$

$c_{d_o}$ minimum section drag coefficient, $\frac{\text{minimum drag}}{q_\infty c}$

$c_l$ section lift coefficient, $\frac{\text{lift}}{q_\infty c}$

$c_l'$ lift-coefficient component, $\frac{\text{lift component}}{q_\infty R}$

$c_m$ section pitching-moment coefficient, $\frac{\text{pitching moment}}{q_\infty c^2}$ (moment about $x' = 0.4\ c$)

$c_{m'}$ pitching-moment coefficient component, $\frac{\text{pitching-moment component}}{q_\infty R^2}$ (moment about leading-edge radius center line)

$c_n$ section normal-force coefficient, $\frac{\text{normal force}}{q_\infty c}$

$c_r$ section resultant-force coefficient, $\frac{\text{resultant force}}{q_\infty c}$

D drag

L lift

M Mach number

p static pressure

q dynamic pressure

R nose radius

x wind-axis coordinate

x' body-axis coordinate

$\tilde{x}'$ center of pressure of windward wedge surface (eq. (18))

$\alpha$ angle of attack

$\gamma$ ratio of specific heats

$\delta$ flow deflection angle

$\delta_w$ wedge angle

$\theta$ shock-wave angle

$\omega$ surface inclination, $\omega = \alpha + \delta_w$

Subscripts

D detachment

$l$ lower surface

| | |
|---|---|
| le | leading edge |
| max | maximum value |
| $\infty$ | free stream |
| st | stagnation |
| u | upper surface |

Superscripts

| | |
|---|---|
| ~ | aerodynamic parameters obtained from oblique-shock theory |
| – | correlation parameters (eqs. (24), (25), (26), and (27)) |

## NUMERICAL BLUNT-WEDGE SOLUTIONS

### Method and Results of Numerical Calculations

The inviscid hypersonic pressure distributions for circularly blunt wedges have been obtained by numerical solution of the ideal gas equations on an IBM 7090 computer for a range of wedge angles. The flow over the blunt leading edge was computed by the inverse method of reference 4 which is an extension to plane flows of the inverse numerical method of reference 5.

The solutions for blunt leading edges provided the supersonic values along the line of inputs for continuing the computations over the wedge surfaces by the numerical method of charcteristics. The line of inputs and other features of the flow are indicated in sketch (a). The procedure was essentially the same as that of reference 6 with the exception that a quadratic rather than linear interpolation of entropy was used. A quadratic interpolation of entropy was found necessary to account for the correct entropy layer due to the blunt leading edge at large distances downstream. As a result of this interpolation scheme, the mass flow within the shock layer was in close agreement with that of the free stream at all streamwise positions. To reduce the computing time, 12 inputs were used rather than the 25 of reference 6, since the number of inputs was found to have a negligible effect on the accuracy of the results.

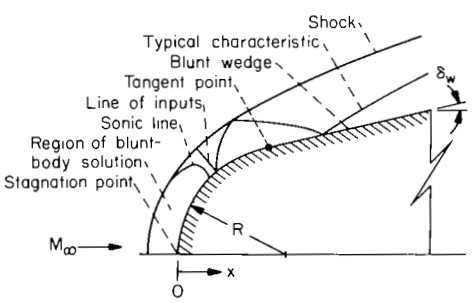


Sketch (a)

The solutions were obtained for as wide a variation in wedge angle as the computing procedure would permit. Solutions were obtained for wedge angles up to $30^\circ$ which were within the range where the flow was entirely supersonic over the wedge surface. The absence of solutions for greater angles is of little concern because at the higher angles, induced effects of the blunt leading edge are small and surface pressure is closely predicted by oblique-shock theory. The lower limits of wedge angles of $-15^\circ$ and $-5^\circ$ for specific-heat ratios of 1.400 and 1.667, respectively, are imposed because of inaccuracies in the blunt-body solution for inputs near the body.

Pressure distributions over blunt leading edges.- The effects of specific-heat ratio on the pressure distribution of the leading edge are shown in figure 1. Since characteristic solutions could not be obtained for a specific-heat ratio of 1.0 at Mach numbers of 10 and $\infty$, only the subsonic blunt leading-edge part of the solution is shown in figure 1(a). The pressure distribution for $\gamma$ of 1.0 and infinite Mach number (fig. 1(b)) was obtained by the Newton-Busemann pressure law (Newtonian plus centrifugal force correction) given in reference 3 and under these conditions is an exact solution. For specific-heat ratios of 1.400 and 1.667, the characteristics part of the solution begins slightly after the sonic point at $x/R \cong 0.3$ and continues to $x/R = 1.0$. The shape of the solution for $\gamma$ of 1.667 suggests slight inaccuracies in the blunt-body solution which are adjusted as the characteristic solution proceeds. The effect of specific-heat ratio for the range from 1.200 to 1.667 is small. Although not shown, modified Newtonian theory, $C_p = C_{p_{st}} \sin^2 \delta$, closely predicts the pressure distribution over the forward part of the nose ($x/R \lesssim 0.4$), but seriously underestimates the pressures over the afterpart ($x/R \gtrsim 0.4$). For these pressures reference 7 gives a better estimate which consists in matching pressure gradients obtained from modified Newtonian theory and a Prandtl-Meyer expansion.

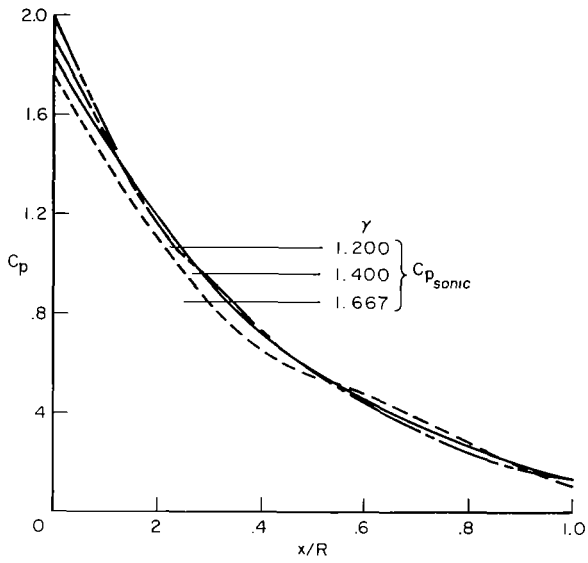


(a) $M_\infty = 10$

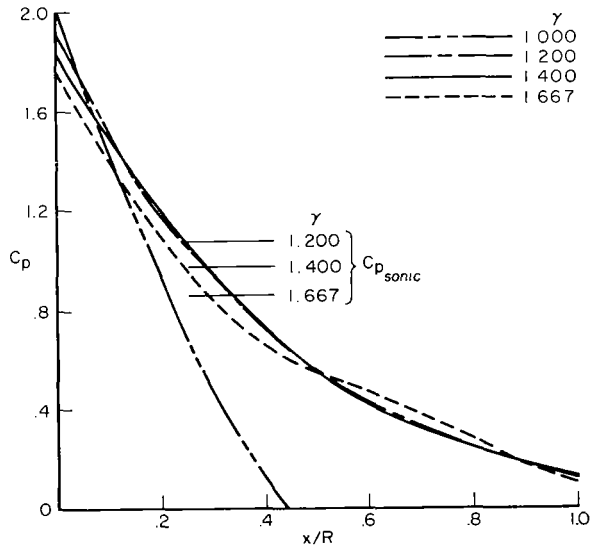


(b) $M_\infty = \infty$

Figure 1.- Pressure distribution over the blunt leading edge.

Pressure distribution over a blunt wedge.- The effects of wedge angle and specific-heat ratio on the pressure distributions over the surfaces of blunt wedges are presented in figure 2 for two Mach numbers. In general, the pressure distributions decay exponentially, that is, the maximum pressures at or near the tangent points decay to the sharp-wedge value. Increasing the wedge angle reduces the extent of the decay and for an angle of 30° the decay is relatively unimportant. The solutions of figure 2 for $\gamma = 1.667$ and a 30° wedge indicate a steep compression starting at the tangent point similar to an imbedded shock. Except for small wedge angles, changing Mach number from 10 to $\infty$ (fig. 2) decreased the pressure coefficient consistent with sharp-wedge theory. However, because of the induced effects of bluntness, this trend was reversed at small wedge angles. The pressure distributions of figure 2 are presented in more detail in charts 1 and 2 at the end of the report.

A comparison of the wedge-surface maximum pressure coefficients from figure 2 with sharp-wedge values is shown in figure 3 for $M_\infty = \infty$. The

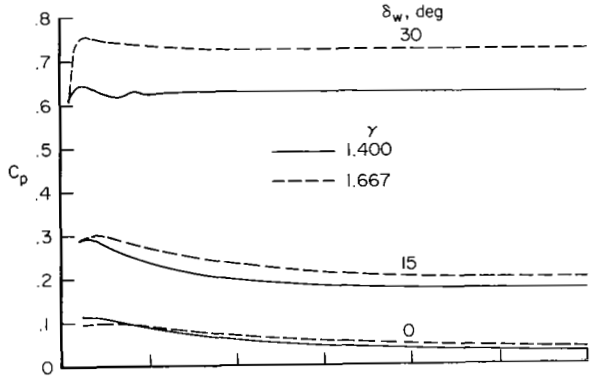


(a) $M_\infty = 10$

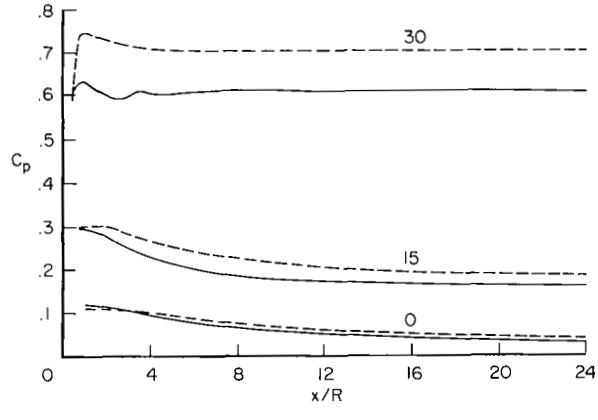


(b) $M_\infty = \infty$

Figure 2.- Pressure distribution over the blunt-wedge surface for specific-heat ratios of 1.400 and 1.667.

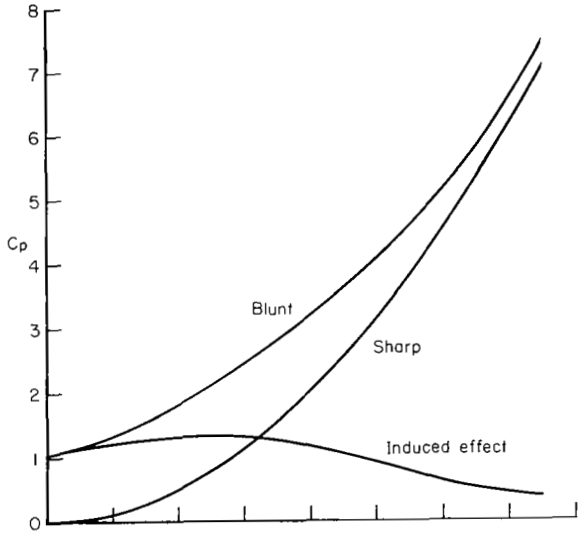


(a) $\gamma = 1.667$

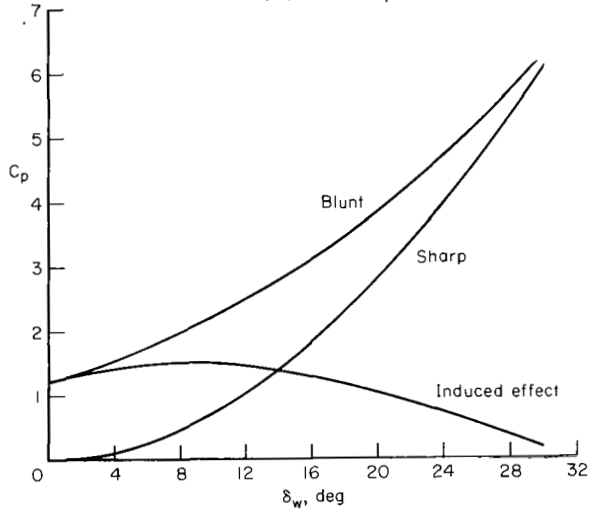


(b) $\gamma = 1.400$

Figure 3.- Comparison of maximum induced pressure coefficient of blunt wedges with sharp-wedge theory; $M_\infty = \infty$.

magnitude and relative importance of the induced effects of bluntness are indicated by the difference between the maximum pressure coefficients of the blunt and sharp wedges. It is apparent that induced effects are relatively unimportant for large wedge angles. For wedge angles less than about $26^{\circ}$, induced effects are slightly less for $\gamma$ of 1.667 than for 1.400.

## AIRFOIL-SECTION CHARACTERISTICS

The pressure distributions for the blunt wedges have been integrated graphically to provide the contributions to lift, drag, and pitching-moment coefficients of the leading-edge and wedge surfaces. A method will be developed for evaluating characteristics of blunt airfoils at angle of attack by the superposition of the blunt-wedge solutions separately obtained for the upper and lower surfaces.

### Superposition of Blunt-Wedge Solutions

Figure 4 presents the components of lift coefficient and of drag coefficient contributed by the segments of the leading edge between the stagnation point and the upper or lower tangent points (see sketch (a)). The dashed portions of the curves were obtained from extrapolations of pressure distributions. The results are applicable for Mach numbers from 10 to $\infty$ since the effect of Mach number is negligible. It is noted from figure 4 that the lift and drag for $x/R$ greater than 1.0 increases very little so that contributions to lift and drag of surfaces that do not "see" the flow are small.

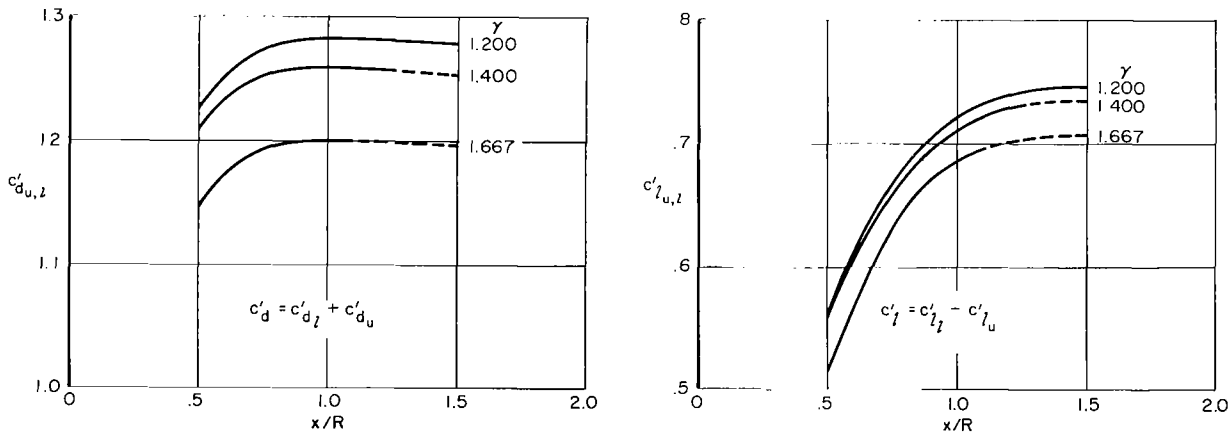


(a) Component of drag coefficient.

(b) Component of lift coefficient.

Figure 4.- Components of lift and drag coefficients for the upper or lower segments of the blunt leading edge for Mach numbers from 10 to $\infty$.

The respective contributions of the leading-edge and wedge surfaces have been combined to provide universal charts from which inviscid lift, drag, and pitching-moment coefficients of circularly blunt-wedge airfoils can be easily evaluated. These results are presented in charts 3 through 8 for specific-heat ratios of 1.400 and 1.667. For upper-surface inclinations greater than $15^\circ$ ($\gamma = 1.400$) and greater than $5^\circ$ ($\gamma = 1.667$) the curves of the charts were obtained from extrapolations of pressure distributions as previously noted. Since the pressure coefficient is rapidly approaching the limiting value, $-2/\gamma M_\infty^2$, with increasing upper-surface inclination, the need for extrapolations diminishes with increasing angles of attack.

Coordinate transformation and use of charts.- Because the force contributions are presented as lift and drag coefficients, a coordinate transformation from the body axis to the wind axis of the blunt-wedge solutions is required. Equations (1) and (2) are the coordinate transformations of the trailing edges of the upper and lower surfaces when inclined at an angle, $\omega$, to the wind axis (sketch (b)).

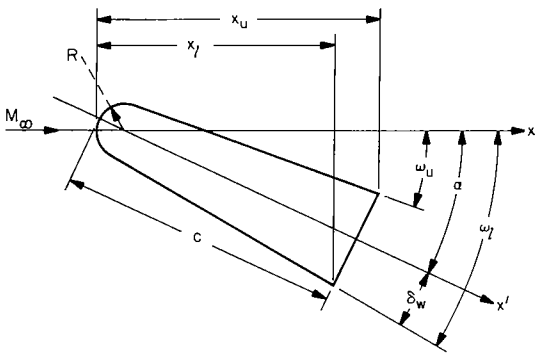


Sketch (b)

$$x_u = \frac{c + R(\sin \alpha / \cos \omega_u) - R}{\cos \alpha + \sin \alpha \tan \omega_u} + R \qquad (1)$$

$$x_l = \frac{c - R(\sin \alpha / \cos \omega_l) - R}{\cos \alpha + \sin \alpha \tan \omega_l} + R \qquad (2)$$

To estimate the lift, drag, and pitching moments for a particular blunt-wedge airfoil, it is first necessary to evaluate the inclinations and the trailing-edge coordinates of the upper and lower surfaces for each angle of attack being considered. The contributions $c_l'$, $c_d'$, and $c_m'$ of the upper and lower surfaces may then be read directly from charts 3 through 8. To facilitate making this transformation, equations (1) and (2) are presented as curves in chart 9. The procedure is illustrated by the arrows on the transformation and airfoil design charts for a typical airfoil having $c/R = 15$, $\delta_w = 5^\circ$, and $\alpha = 25^\circ$. In the preparation of these charts the upper and lower surfaces originate at the stagnation point and not at the leading edge of the airfoil. The contribution of the upper surface is added to the lower surface to evaluate the total drag coefficient but it is subtracted from the lower surface contribution to evaluate the total lift and pitching-moment coefficients. After evaluating the total force and moment coefficients, conversion to the more conventional airfoil coefficients based on chord can be made by multiplying by the appropriate $R/c$ ratio.

## Effects of Airfoil Geometry

Two parameters that define the profile of circularly blunt airfoils are the bluntness ratio, R/c, and the wedge angles, $\delta_w$, of the upper and the lower surfaces with respect to the body or reference axis. Since variations of either parameter may have important effects on aerodynamic characteristics, the effects of varying each will be considered separately. Only the symmetrical airfoil will be considered, since it is apparent the effect of asymmetry can be accounted for by a shift in reference angle of attack. A base pressure coefficient of zero will be assumed.

Effect of wedge angle.- Figure 5 presents the effect of wedge angle on the lift, drag, and pitching-moment coefficients and lift-drag ratio of blunt airfoils having a bluntness, R/c, of 0.05. At hypersonic Mach numbers, it is evident from figure 5 that increasing the wedge angle is an effective means for increasing lift-curve slope of blunt airfoils within the angle-of-attack range shown. It may be observed that the lift curve of the blunt airfoil of $0^\circ$ wedge angle is well approximated by oblique-shock flat-plate theory at the higher angles of attack. Although increasing wedge angle increased the drag coefficient, the maximum value of lift-drag ratio was practically unaffected because of the accompanying increase in lift coefficient; however, the angle of attack for maximum lift-drag ratio was reduced. For a given angle of attack, pitching-moment coefficient increased with wedge angle. Because of a corresponding increase in lift coefficient, however, increasing the wedge angle increased the static longitudinal stability, $-(dc_m/dc_l)$, only slightly.

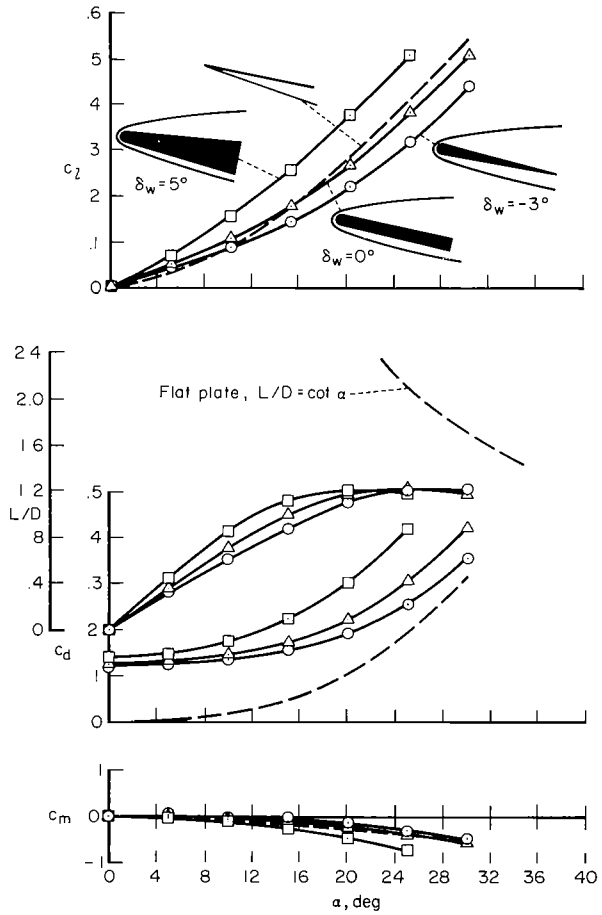


(a) $M_\infty = 10$, $\gamma = 1.400$

Figure 5.- Effect of varying wedge angle on the aerodynamic characteristics of blunt airfoils; R/c = 0.05.

Effect of varying bluntness.- Leading-edge bluntness may be considered to exert three influences on the aerodynamic characteristics of wedge airfoils. First, the pressures on the leading edge differ from those of a sharp airfoil and effectively cause concentrated forces at the leading edge. Second, bluntness has a carry-over or

induced effect on the pressure distribution over the flat aftersurfaces of the airfoil. Thirdly, bluntness causes a foreshortening of the effective chord over which the oblique-shock pressures predominate. While these effects cannot be separated readily, their separate effects can be observed at certain angles of attack and will be demonstrated by figures 5 and 6. As shown in figure 6, the first influence of bluntness produces a large increase of drag at $0^{\circ}$ angle of attack. Although not readily apparent, the drag increase is accompanied by a small loss in lift that develops with increasing angle of attack. The loss in lift is due to an unbalance of pressure forces acting on the leading-edge surfaces between the stagnation point and the upper and lower tangent points. The second or induced effect of bluntness is demonstrated by the increased lift of the blunt airfoil of $0^{\circ}$ wedge angle relative to that of the flat plate in the lower angle-of-attack range of figure 5. The third effect of bluntness is demonstrated by the loss in lift of the blunter airfoils at high angles of attack of figure 6.

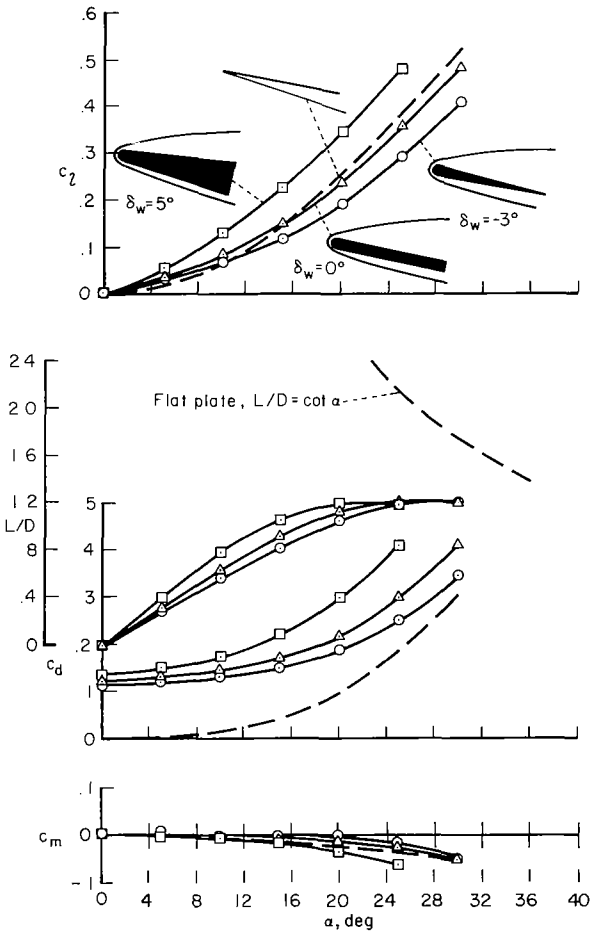


(b) $M_\infty = \infty$, $\gamma = 1.400$

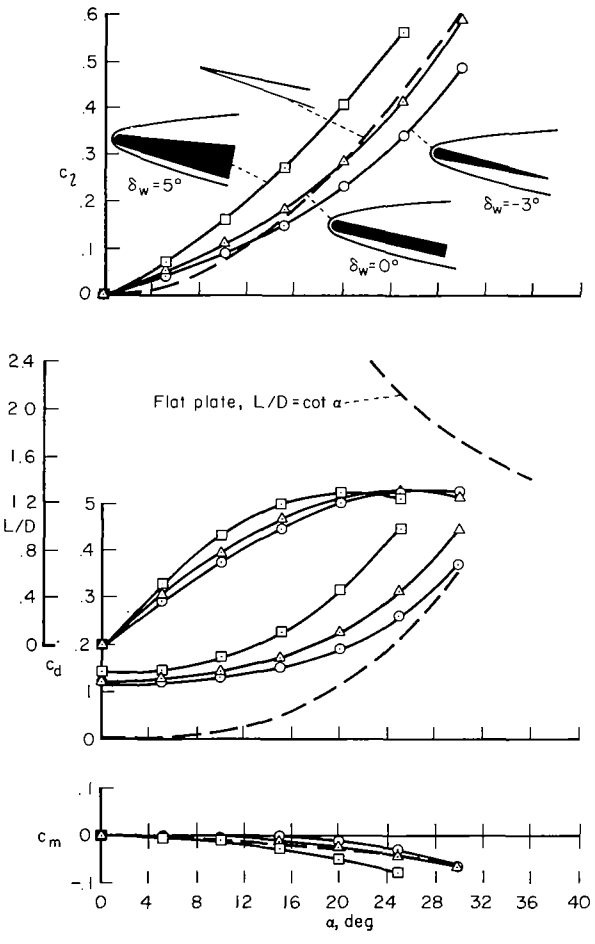


(c) $M_\infty = \infty$, $\gamma = 1.667$

Figure 5.- Concluded.

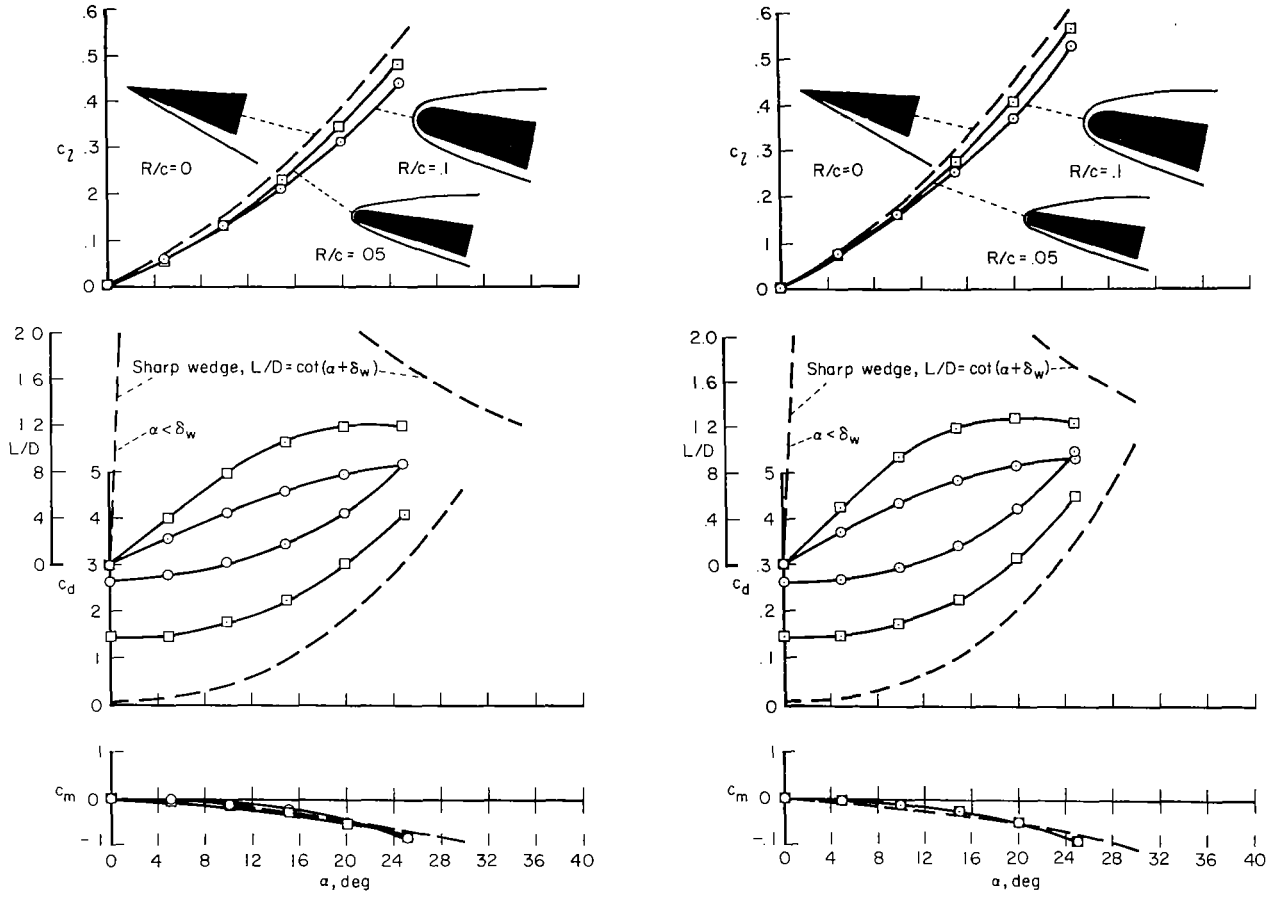


(a) $M_\infty = \infty$, $\gamma = 1.400$

(b) $M_\infty = \infty$, $\gamma = 1.667$

Figure 6.- Effect of varying bluntness on the aerodynamic characteristics of blunt airfoils; $\delta_w = 5^\circ$.

In general, induced effects of bluntness are important only for airfoils of small wedge angle at small angles of attack and are overpowered by oblique-shock effects for wedge angles of at least $5^\circ$ or greater at all angles of attack. At higher angles of attack, where induced effects are small, the loss in lift due to increasing bluntness is approximately proportional to R/c. Increasing bluntness was accompanied by increased drag and a reduction in lift-drag ratio. The variation of pitching-moment coefficient with angle of attack was only slightly affected by increasing bluntness. Evidently, the contribution of nose drag to pitching moment was largely compensated by an opposing moment due to loss in lift of the nose. It should be noted that this balance between nose-lift and nose-drag moment contributions is a characteristic of the circular blunt nose and may not exist for other types of bluntness.

Effect of Mach number and specific-heat ratio.- Figures 5(a) and 5(b) indicate that increasing Mach numbers from 10 to $\infty$ reduced the lift and drag, but left maximum lift-drag ratio about the same. Increasing specific-heat ratio from 1.400 to 1.667 (figs. 5(b) and 5(c)) increased the lift and maximum lift-drag ratio. Similar effects due to increasing the specific-heat ratio are evident in figures 6(a) and 6(b) for an airfoil whose bluntness is 0.10. Figures 5 and 6 also demonstrate that increasing the specific-heat ratio increased the pitching-moment coefficient, but because of the increase in lift coefficient, the static stability, $-(dc_m/dc_l)$, is relatively unaffected. In conclusion, it has been demonstrated that induced effects of bluntness are important mainly at low angles of attack. At high angles of attack, oblique-shock theory of sharp-wedge airfoils correctly predicts for circularly blunt airfoils the trends of lift coefficient produced by increasing wedge angle, Mach number, and specific-heat ratio. Because of its general suitability for predicting these trends, oblique-shock theory will be examined next with the intention of developing a simple approximation that accurately predicts blunt airfoil characteristics at hypersonic Mach numbers.

## HYPERSONIC WEDGE THEORY

### Derivation and Application

The practical application of oblique-shock theory is severely encumbered by the implicit relation that exists between shock angle, deflection angle, Mach number, and specific-heat ratio as given by the cubic equation in $\sin^2\theta$ of reference 8,

$$\sin^6\theta - \left[\left(\frac{M_\infty^2 + 2}{M_\infty^2}\right) + \gamma \sin^2\delta\right]\sin^4\theta + \left\{\left(\frac{2M_\infty^2 + 1}{M_\infty^4}\right) + \left[\frac{(\gamma+1)^2}{4} + \frac{\gamma - 1}{M_\infty^2}\right]\sin^2\delta\right\}\sin^2\theta - \frac{\cos^2\delta}{M_\infty^4} = 0 \tag{3}$$

At hypersonic Mach numbers, it is possible, by an order of magnitude analysis, to derive approximate explicit equations for shock angle and pressure coefficient as a function of deflection angle, Mach number, and specific-heat ratio that in the limit, $M_\infty = \infty$, are exact.

If terms of order $1/M_\infty^4$ are neglected compared to terms of order $1/M_\infty^2$, equation (3) reduces to a simple quadratic equation in terms of the variable, $\sin^2\theta$, whose solution is

$$\sin^2\theta = \frac{1}{2}\left(1 + \frac{2}{M_\infty^2} + \gamma\sin^2\delta \pm \cos\delta\sqrt{1 - \frac{4}{M_\infty^2} - \gamma^2\sin^2\delta}\right) \tag{4}$$

and since

$$C_p = \frac{4}{\gamma + 1}\left(\sin^2 \theta - \frac{1}{M_\infty{}^2}\right) \tag{5}$$

it follows that

$$C_p = \frac{2}{\gamma + 1}\left(1 + \gamma \sin^2 \delta \pm \cos \delta \sqrt{1 - \frac{4}{M_\infty{}^2} - \gamma^2 \sin^2 \delta}\right) \tag{6}$$

The positive and negative signs before the radicals of equations (4) and (6) constitute the strong and weak shock solutions, respectively. If $M_\infty = \infty$, equations (4) and (6) reduce to the exact results

$$\sin^2 \theta = \frac{1}{2}\left(1 + \gamma \sin^2 \delta \pm \cos \delta \sqrt{1 - \gamma^2 \sin^2 \delta}\right) \tag{7}$$

$$C_p = \frac{2}{\gamma + 1}\left(1 + \gamma \sin^2 \delta \pm \cos \delta \sqrt{1 - \gamma^2 \sin^2 \delta}\right) \tag{8}$$

and, in the Newtonian limit of $M_\infty = \infty$, and $\gamma = 1$, simplify to the Newtonian values

$$\theta = \pi/2$$

$$\theta = \delta$$

and

$$C_p = 2$$

$$C_p = 2 \sin^2 \delta$$

which represent the strong and weak shock solutions, respectively.

Conditions for shock detachment are closely approximated by equating the radical in equation (4) to zero, giving

$$\sin^2 \theta_D = \frac{1}{2} + \frac{1}{2}\left(\frac{2}{M_\infty{}^2} + \frac{M_\infty{}^2 - 4}{\gamma M_\infty{}^2}\right) \tag{9}$$

$$\sin^2 \delta_D = \frac{1 - (4/M_\infty{}^2)}{\gamma^2} \tag{10}$$

and

$$C_{p_D} = \frac{2}{\gamma}\left[\frac{\gamma + 1 - (4/M_\infty{}^2)}{\gamma + 1}\right] \tag{11}$$

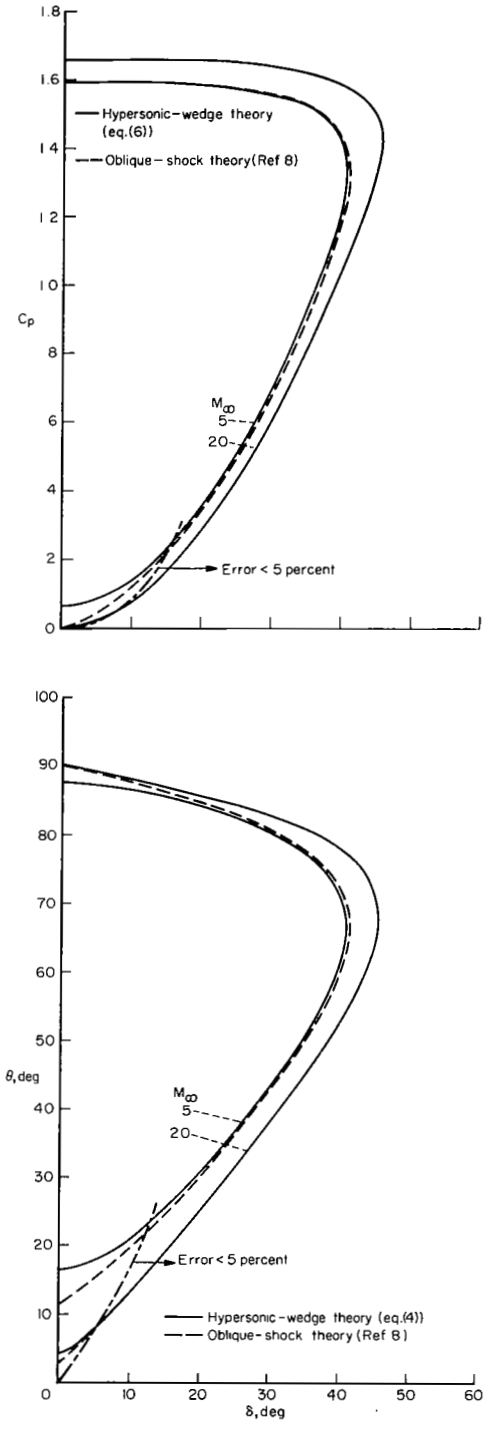


Figure 7.- Comparison of oblique-shock solutions with hypersonic wedge theory; $\gamma = 1.400$.

For infinite Mach number, exact detachment conditions are

$$\sin \theta_D = \sqrt{\frac{\gamma + 1}{2\gamma}} \qquad (12)$$

$$\sin \delta_D = 1/\gamma \qquad (13)$$

$$C_{p_D} = 2/\gamma \qquad (14)$$

These results constitute an explicit hypersonic wedge theory of oblique shocks. The oblique-shock problem has been considered also in reference 9 with an analysis that parallels small disturbance theory. The equations derived in reference 9, while useful, are cumbersome to apply and the exact solution at infinite Mach number is not achieved.

Figure 7 presents a comparison of equations (4) and (6) with exact solutions of the oblique shock equation (3) in order to demonstrate the applicability of the present theory. The accuracy and the range of deflection angles for which the theory is applicable improves with increasing Mach number, as indicated by the error boundary of figure 7. Figure 7 demonstrates that the theory can hardly be distinguished from the exact curves at a Mach number of 20 for deflection angles greater than about $10^\circ$.

The present hypersonic wedge theory complements the small-disturbance theory of references 1 and 10 for deflection angles greater than about $12^\circ$ (where small disturbance theory is no longer valid) as is shown in figure 8. The judicious use of both theories permits rapid and accurate predictions of oblique-shock properties at all hypersonic Mach numbers. Figure 8 calls attention to the inability of Newtonian theory to accurately predict pressure coefficients or the detachment of oblique shocks for Mach numbers other than $\infty$, even if the specific-heat ratio is 1.0.

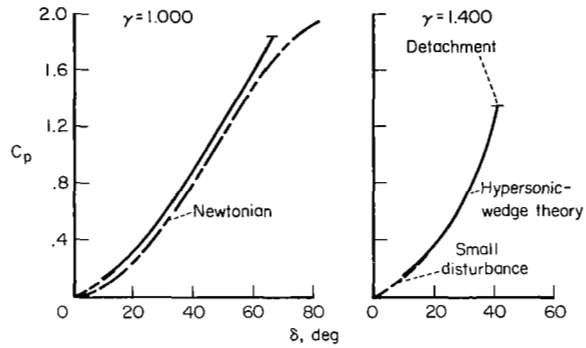


Figure 8.- Comparison of wedge theories for a Mach number of 5.

The significant effects of specific-heat ratio on oblique-shock characteristics are demonstrated by the exact solutions of figure 9 for infinite Mach number. If the specific-heat ratio is 1.0, the weak-shock solution reduces to Newtonian theory, while the strong-shock solution yields a pressure coefficient of 2 consistent with the normal-shock solution. Simple relations are shown (fig. 9) for the pressure coefficient and shock-wave angle for detachment for any specific-heat ratio.

The application of equation (6) with tangent-wedge approximations provides a method for rapidly estimating the pressure distributions of sharp, curved airfoils at angle of attack. The accuracy of this method is comparable to that of the shock-expansion theory, but the present method is more rapid.

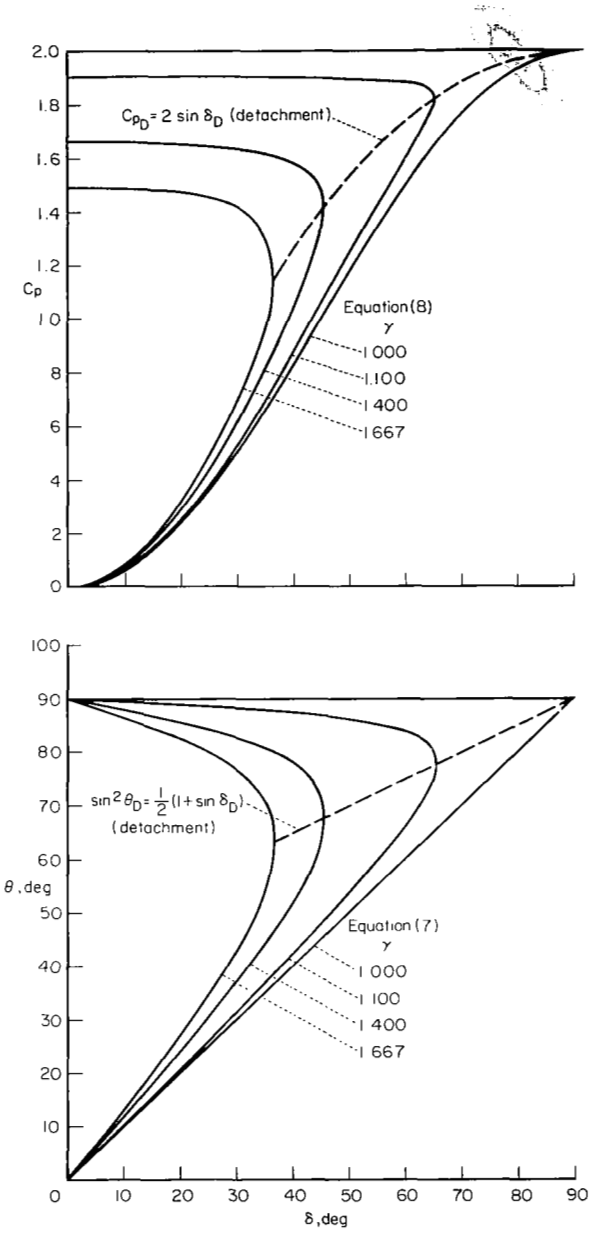


Figure 9.- Effect of specific-heat ratio on exact pressure coefficients and shock-wave angles predicted by hypersonic wedge theory; $M_\infty = \infty$.

## Development of Correlation Parameters

$M_\infty = \infty$ and $\gamma = 1.0$.- Since the sharp airfoil can be considered the limiting case as airfoil bluntness decreases to zero, the question arises as to what extent sharp-airfoil theory is useful for predicting aerodynamic

characteristics of blunt airfoils. For the Newtonian limit of $M_\infty = \infty$ and $\gamma = 1.0$, the relationship is simple and well understood. For these conditions, the Newton-Busemann pressure law predicts that the flow separates from the circular leading edge at an angle of $54.7^\circ$ from the stagnation point ($x/R = 0.422$) and the pressure coefficient is zero until the flow "sees" the flat surfaces of the airfoil (see ref. 11). The pressure coefficient of the flat surface is given by $C_p = 2 \sin^2 \omega$. For $M_\infty = \infty$ and $\gamma = 1$, the circular leading edge contributes to the drag but not to the lift of the airfoil for a wide range of angles of attack. These concepts when applied to blunt airfoils (provided $\alpha > \delta_w$) give the following equations,

$$c_l = C_p \cos(\alpha + \delta_w) \left[ \frac{1 - \frac{R}{c}(1 - \sin \delta_w)}{\cos \delta_w} \right] \tag{15}$$

$$\left(c_d - c_{d_{le}}\right) = C_p \sin(\alpha + \delta_w) \left[ \frac{1 - \frac{R}{c}(1 - \sin \delta_w)}{\cos \delta_w} \right] \tag{16}$$

$$\left[ c_m - \left(\frac{x'}{c} - \frac{R}{c}\right) c_{d_{le}} \sin \alpha \right] = C_p \cos \delta_w \left(\frac{x'}{c} - \frac{\tilde{x}'}{c}\right) \left[ \frac{1 - \frac{R}{c}(1 - \sin \delta_w)}{\cos \delta_w} \right] \tag{17}$$

$$\frac{\tilde{x}'}{c} = \frac{R}{c} + \frac{1}{2 \cos \delta_w} \left[ \frac{1 - \frac{R}{c}(1 - \sin \delta_w)}{\cos \delta_w} \right] \tag{18}$$

where

$$C_p = 2 \sin^2(\alpha + \delta_w) \tag{19}$$

and $x'/c$ is the moment reference center. As an aid to interpreting the equations, the airfoil forces and geometry are shown in sketch (c).

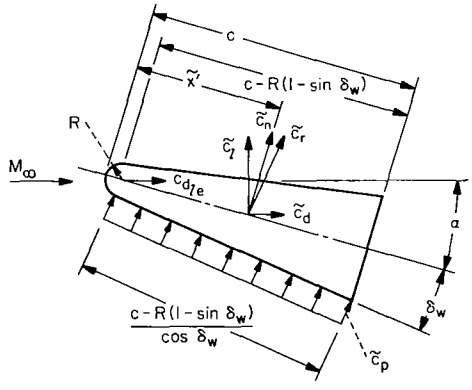


Sketch (c)

In summary, equations (15) through (19) represent exact asymptotic solutions of the aerodynamic properties of any circularly blunt- or sharp-wedge airfoil in the Newtonian limit $M_\infty = \infty$ and $\gamma = 1.0$. The sharp-wedge solutions are, of course, special cases for which $R/c$ and $c_{d_{le}}$ are zero. Although equations (15) through (19) are mainly of academic interest, by suitable modifications they can be applied to the more practical case of $M_\infty < \infty$ and $\gamma > 1.0$. These modifications will now be made.

$M_\infty < \infty$ and $\gamma > 1.0$.- Departure from the Newtonian limit introduces three effects which must be considered. In order of increasing importance these effects are: (1) a negative lift contribution of the leading edge, (2) induced effects of bluntness on the flat surfaces of the airfoil, and (3) the fact that $2 \sin^2 \omega$ is a relatively poor estimate of the correct level of pressure coefficient on the flat windward surface. These differences from the Newtonian limit are illustrated by sketch (d).

Since it has been previously demonstrated (fig. 3) that induced effects are important mainly at small flow deflections, no correction for induced effects will be made. Correcting equations (15) and (17) for lift of the leading edge and using equation (6) with $\delta$ replaced by $\alpha + \delta_w$ rather than equation (19) gives the modified equations

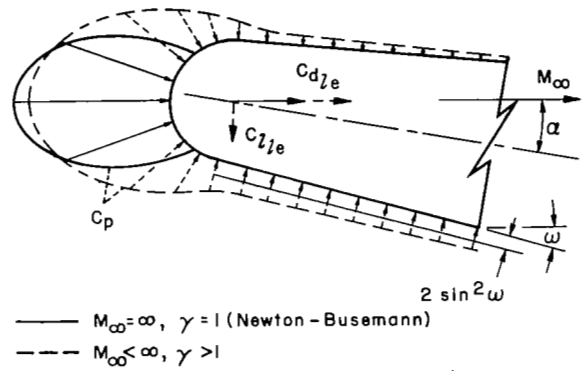


Sketch (d)

$$\left(c_l - c_{l_{le}}\right) = C_p \cos(\alpha + \delta_w) \left[\frac{1 - \frac{R}{c}(1 - \sin \delta_w)}{\cos \delta_w}\right] \tag{20}$$

$$\left(c_d - c_{d_{le}}\right) = C_p \sin(\alpha + \delta_w) \left[\frac{1 - \frac{R}{c}(1 - \sin \delta_w)}{\cos \delta_w}\right] \tag{21}$$

$$\left[c_m - \left(\frac{x'}{c} - \frac{R}{c}\right)\left(c_{l_{le}} \cos \alpha + c_{d_{le}} \sin \alpha\right)\right] = C_p \cos \delta_w \left(\frac{x'}{c} - \frac{\tilde{x}'}{c}\right) \left[\frac{1 - \frac{R}{c}(1 - \sin \delta_w)}{\cos \delta_w}\right] \tag{22}$$

and

$$C_p = \frac{2}{\gamma + 1}\left[1 + \gamma \sin^2(\alpha + \delta_w) - \cos(\alpha + \delta_w)\sqrt{1 - \frac{4}{M_\infty^2} - \gamma^2 \sin^2(\alpha + \delta_w)}\right] \tag{23}$$

These equations can be put in a form more suitable for correlating the numerical solutions by defining the correlating parameters

$$\bar{c}_l \equiv \left(c_l - c_{l_{le}}\right)\left[\frac{\cos \delta_w}{1 - \frac{R}{c}(1 - \sin \delta_w)}\right] = \bar{C}_p \tag{24}$$

$$\bar{c}_d \equiv \left(c_d - c_{d_{le}}\right)\left[\frac{\cos \delta_w}{1 - \frac{R}{c}(1 - \sin \delta_w)}\right] \cot(\alpha + \delta_w) = \bar{C}_p \tag{25}$$

$$\bar{c}_m \equiv \frac{\left[c_m - \left(\frac{x'}{c} - \frac{R}{c}\right)\left(c_{l_{le}} \cos \alpha + c_{d_{le}} \sin \alpha\right)\right]}{\left(\frac{x'}{c} - \frac{\tilde{x}'}{c}\right)}\left[\frac{\cos \delta_w}{1 - \frac{R}{c}(1 - \sin \delta_w)}\right]\frac{\cos(\alpha + \delta_w)}{\cos \delta_w} = \bar{C}_p \tag{26}$$

and

$$\bar{C}_p \equiv C_p \cos(\alpha + \delta_w) \tag{27}$$

It may be observed that $\bar{C}_p$ is the lift coefficient of a flat plate inclined at an angle, $\alpha + \delta_w$ (upper surface expansion neglected).

Lift-curve slope, $dc_l/d\alpha$, and longitudinal stablity, $-(dc_m/d\alpha)$, may be estimated from equations (20), (22), and (23) by differentiation, considering $c_l$ and $c_m$ as dependent variables and $\alpha$ as the independent variable.

The numerical solutions for the lift, drag, and pitching-moment coefficients of figures 5 and 6 are correlated by these parameters in figure 10. With the exception of low angles of deflection, where induced effects are important and where theory does not apply for finite Mach numbers, excellent correlation is demonstrated for a variety of airfoils and flow conditions. The effects of wide variations in Mach number and specific-heat ratio are well correlated for the angle-of-attack range wherein maximum lift-drag ratio is likely to occur. Even for the blunter airfoils, for which $R/c > 0.05$ (fig. 10(b)) and for which induced effects are more important, good correlation is retained.

From these results, it is evident that the induced effects of bluntness on the pressure distribution of the upper and lower airfoil surfaces are largely self-compensating and hypersonic wedge theory (eq. (6)) closely accounts for integrated forces and moments. To demonstrate this more clearly, a single computation using Newtonian theory (eq. (19)) in place of hypersonic wedge theory is shown in figure 10(a). The deviation from perfect correlation of lift coefficient is about 20 percent if Newtonian theory is used as compared to about 2 percent for hypersonic wedge theory.

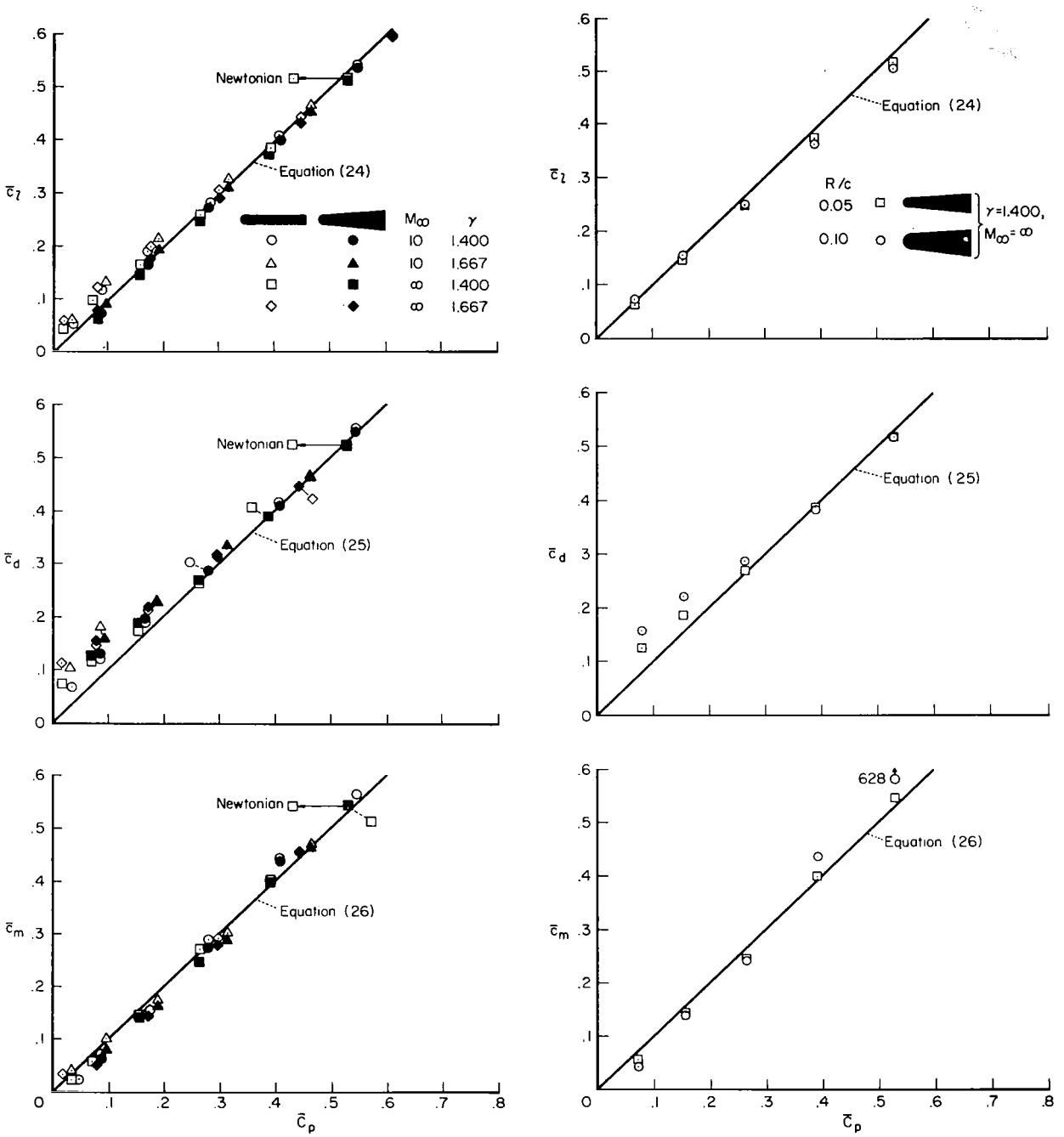


(a) Effect of wedge angle.

(b) Effect of bluntness.

Figure 10.- Correlation of aerodynamic coefficients of blunt airfoils evaluated from characteristic solutions; $\alpha > \delta_w$.

Since induced effects decrease with decreasing Mach number, the correlations are believed applicable for all hypersonic Mach numbers where hypersonic wedge theory is adequate - generally from $M_\infty = 5$ to $\infty$.

Equations (20) through (22) contain the geometrical parameter $[1 - (R/c)(1 - \sin \delta_w)]/\cos \delta_w$. To facilitate rapid estimates of aerodynamic coefficients of blunt airfoils, this parameter is presented in chart 10.

For evaluations of blunt airfoil characteristics (eqs. (24), (25), and (26)) the lift and drag acting on the leading edge may be taken from the numerical solutions presented in figure 4 for gas specific-heat ratios of 1.2, 1.4, and 1.667. These quantities may also be estimated with less accuracy by modified Newtonian theory using the following expressions

$$c_{d_{le}} = \frac{C_{p_{st}}}{c/R}\left[\frac{2}{3} + \cos(\alpha + \delta_w) - \frac{1}{3}\cos^3(\alpha + \delta_w)\right] \tag{28}$$

$$c_{l_{le}} = -\frac{C_{p_{st}}}{3c/R}\sin^3(\alpha + \delta_w) \tag{29}$$

where $\alpha > \delta_w$.

## Prediction of Airfoil Characteristics

Maximum lift coefficient.- The effect of specific-heat ratio on the exact lift curves of flat-plate airfoils at infinite Mach number is presented in figure 11 where

$$c_l = \frac{2}{\gamma + 1}\left(1 + \gamma \sin^2 \alpha - \cos \alpha \sqrt{1 - \gamma^2 \sin^2 \alpha}\right)\cos \alpha \tag{30}$$

Flat-plate lift curves exhibit decidedly nonlinear variations with angle of attack and depart significantly from impact theory as maximum lift coefficient is reached. The lift coefficient at shock detachment increases with increasing $\gamma$, reaches a maximum at $\gamma = \sqrt{2}$, and thereafter decreases with further increase in $\gamma$. It is interesting to note that the maximum lift coefficient corresponds to that for shock detachment for $\gamma$ of about 1.15, but for $\gamma < 1.15$, the maximum lift coefficient occurs well below the angle for shock detachment. These same effects and trends prevail at lower hypersonic Mach numbers, except the curves shift to the left in accordance with the reduction in shock-detachment angle with reduction in Mach number. It should be noted the results presented in figure 11 apply to any sharp-wedge airfoil for $\alpha > \delta_w$ if the origin is shifted a distance $\delta_w$ to the right.

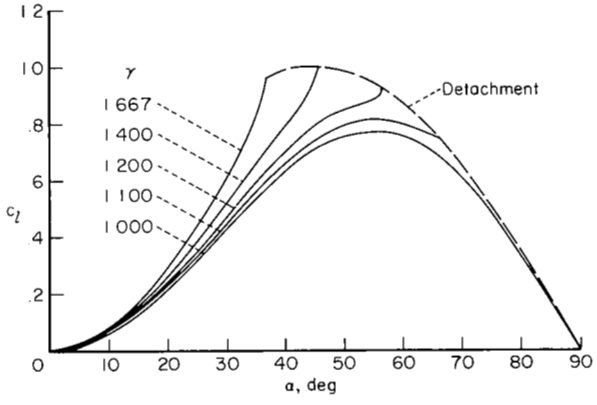


Figure 11.- Effect of specific-heat ratio on the lift characteristics of sharp flat airfoils at infinite Mach number.

The extent to which the flat-plate lift curves of figure 11 near detachment apply to blunt airfoils cannot be determined by numerical solutions. However, because of the close correlation provided by hypersonic wedge theory at high angles of attack (eq. (24) and fig. 10) it is reasonable to expect that the flat-plate solutions predict the trends caused by variations in both specific-heat ratio and Mach number.

Lift-drag ratio.- While it is generally recognized that specific-heat ratio has a small effect on the lift-drag ratio of slender configurations having very small minimum drag coefficients (ref. 12), the effect on blunter shapes has not been clearly established. Since an accurate estimate of maximum lift-drag ratio is essential to predict performance and reentry characteristics of space vehicles, it is worthwhile to examine the equation for lift-drag ratio of flat-plate theory in some detail. The lift-drag ratio at infinite Mach number of a flat-plate airfoil whose minumum drag coefficient is $c_{d_o}$ is given exactly by

$$\frac{L}{D} = \frac{1}{(c_{d_o}/C_p \cos \alpha) + \tan \alpha} \qquad (31)$$

where $C_p$ is a function of the angle of attack and may be obtained from equation (8) with $\delta$ replaced by $\alpha$. An examination of equation (31) shows that as $c_{d_o}$ approaches zero, departures from inviscid flat-plate theory ($L/D = \cot \alpha$) are negligible. Thus the effect of specific-heat ratio through its dependence on pressure coefficient is insignificant. However, if $c_{d_o}$ is sufficiently large, the converse is true and a dependence of $L/D$ on specific-heat ratio is indicated.

Theoretical flat-plate values of maximum lift-drag ratio and the lift coefficient for maximum $L/D$ have been obtained from equations (31) and (8) to show the effect of specific-heat ratio, and the results are presented in figure 12. Values from numerical computations of various blunt airfoils (figs. 5 and 6) with the lift coefficients corrected for loss in lift of the leading edge are shown as data points. Excellent agreement of the blunt-airfoil solutions with flat-plate theory is demonstrated if values are plotted versus minimum drag coefficient. Although the results presented in figure 12 are for infinite Mach number, the maximum lift-drag ratios shown closely approximate those for the Mach number range from about 10 to $\infty$. While the effects of specific-heat

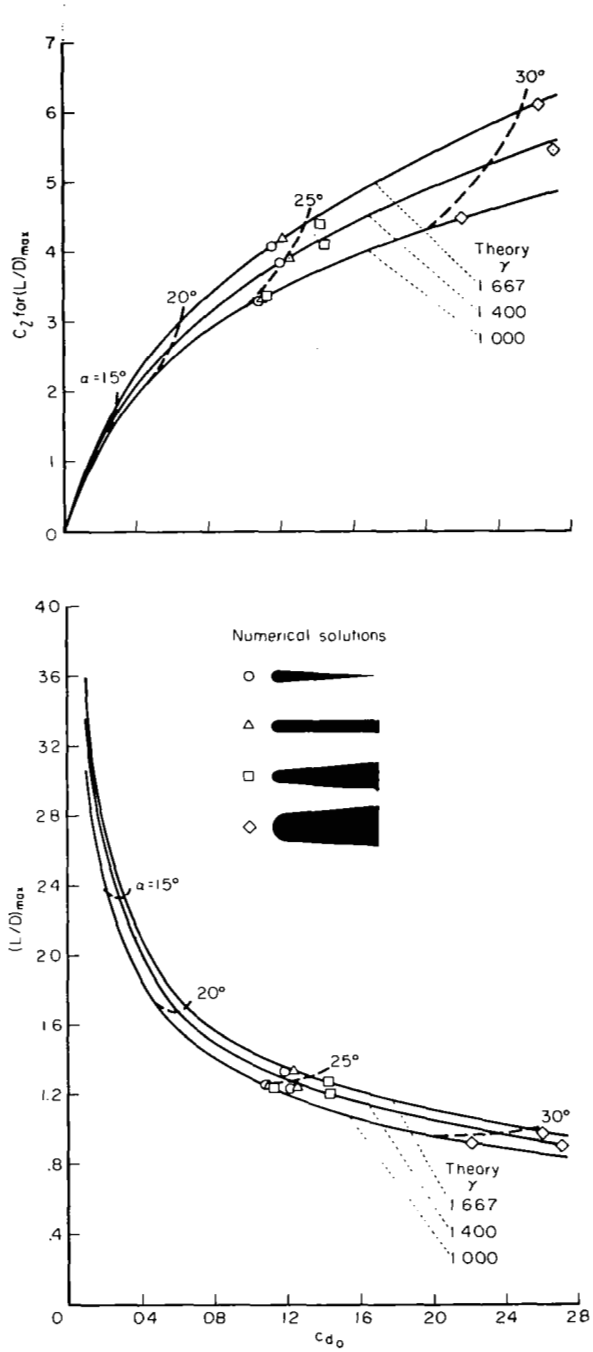


Figure 12.- Effect of specific-heat ratio on the performance parameters of blunt airfoils at hypersonic Mach numbers.

ratio on maximum lift-drag ratio are relatively unimportant for very small minimum drag coefficients, the effect is more important for large values of minimum drag coefficient characterizing blunt airfoils. The large effects of specific-heat ratio on the lift coefficient for maximum lift-drag ratio (fig. 12) are consistent with those shown earlier for the lift curves of both blunt and sharp airfoils (fig. 5). It is readily apparent that Newtonian theory would significantly underestimate both the lift coefficient for maximum lift-drag ratio and the maximum lift-drag ratio.

## CONCLUDING REMARKS

Numerical solutions have been obtained for blunt wedges in a perfect gas. The effects of wedge angle, nose bluntness, and specific-heat ratio have been determined for the Mach number range from 10 to $\infty$. The pressure distributions have been integrated to provide curves from which inviscid lift, drag, and pitching-moment coefficients of circularly blunt-wedge airfoils can be evaluated.

The numerical solutions indicate that increasing the wedge angle of the blunt airfoils significantly increased the lift-curve slope, increased the drag, and had little effect on maximum lift-drag ratio. These trends are consistent with those predicted by oblique-shock theory for sharp airfoils. Increasing the bluntness of the airfoils increased the drag but also caused a loss in lift which developed with increasing angle of attack. The loss in lift was generally proportional to the loss in lift of the leading edge. For wedge angles near $0^{\circ}$, the incorporation of bluntness tended to linearize the lift curves at small angles of attack. The significant effects of increasing gas specific-heat ratio were greater lift-curve slopes and lift-drag ratios.

A hypersonic wedge theory, based on explicit oblique-shock equations, is shown to provide a rapid and accurate prediction of the aerodynamic characteristics of airfoils with attached shocks for any value of the specific-heat ratio. The theory also provides an accurate prediction of conditions at shock detachment for sharp airfoils. For the limiting case of infinite Mach number, the theory is exact for any specific-heat ratio and is in agreement with Newtonian theory for a specific-heat ratio of unity. By accounting for the lift and drag of the leading edge, the theory is shown to be applicable to blunt airfoils for an angle-of-attack range wherein maximum lift-drag ratio occurs. When leading-edge bluntness is taken into account, the theory provides an excellent correlation of the effects of wedge angle, bluntness, and specific-heat ratio at hypersonic Mach numbers. The theory is useful for predicting the maximum lift-drag ratio and the lift coefficient at maximum lift-drag ratio for both blunt and sharp airfoils.

Ames Research Center
National Aeronautics and Space Administration
Moffett Field, Calif., Jan. 14, 1964

## REFERENCES


1. Linnell, Richard D.: Two-Dimensional Airfoils in Hypersonic Flows. Jour. Aero. Sci., vol. 16, no. 1, Jan. 1949, pp. 22-30.

2. Dorrance, William H.: Two-Dimensional Airfoils at Moderate Hypersonic Velocities. Jour. Aero. Sci., vol. 19, no. 9, Sept. 1952, pp. 593-600.

3. Truitt, Robert Wesley: Hypersonic Aerodynamics. Ronald Press, N. Y., 1959.

4. Fuller, Franklyn B.: Numerical Solutions for Supersonic Flow of an Ideal Gas Around Blunt Two-Dimensional Bodies. NASA TN D-791, 1961.

5. Van Dyke, Milton D., and Gordon, Helen D.: Supersonic Flow Past a Family of Blunt Axisymmetric Bodies. NASA TR R-1, 1959.

6. Inouye, Mamoru, and Lomax, Harvard: Comparison of Experimental and Numerical Results for the Flow of a Perfect Gas About Blunt-Nosed Bodies. NASA TN D-1426, 1962.

7. Kaufman, Louis G.: Pressure Estimation Techniques for Hypersonic Flows Over Blunt Bodies. Jour. Astronautical Sci., vol. X, no. 2, 1963, pp. 35-41.

8. Ames Research Staff: Equations, Tables, and Charts for Compressible Flow. NACA Rep. 1135, 1953.

9. Carafoli, Elie: On a Unitary Formula for Compression-Expansion in Supersonic-Hypersonic Flow. Revue DéMecanique Appliquée, vol. 7, no. 5, 1962, pp. 867-876.

10. Van Dyke, Milton D.: A Study of Hypersonic Small-Disturbance Theory. NACA Rep. 1194, 1954.

11. Hayes, Wallace D., and Probstein, Ronald F.: Hypersonic Flow Theory. Academic Press, N. Y., 1959.

12. Love, Eugene S., Henderson, Arthur, Jr., and Bertram, Mitchel H.: Some Aspects of Air-Helium Simulation and Hypersonic Approximations. NASA TN D-49, 1959.

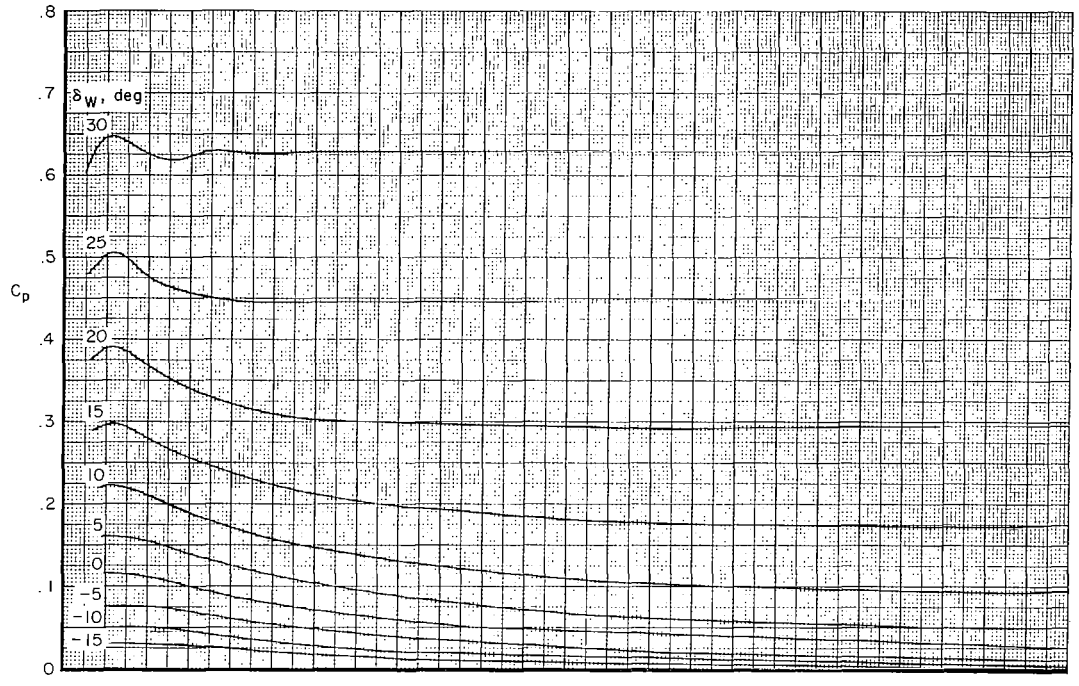


(a) $M_\infty$ - 10

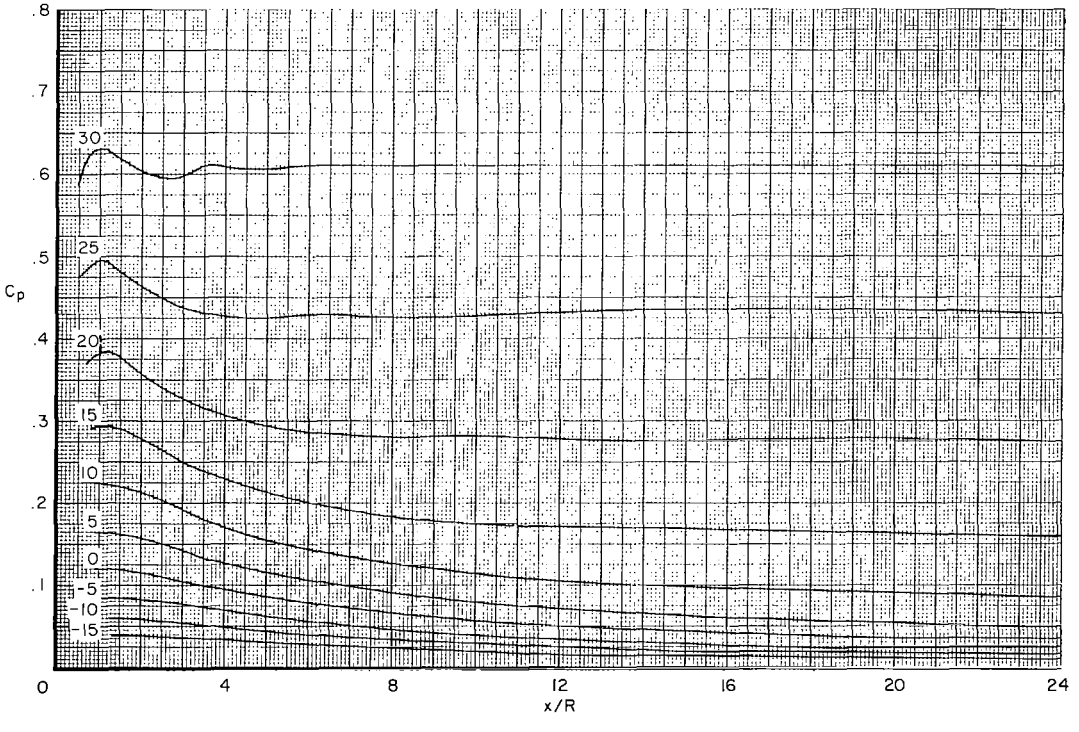


(b) $M_\infty = \infty$

Chart 1.- Pressure distribution over the blunt-wedge surface for a specific-heat ratio of 1.400.

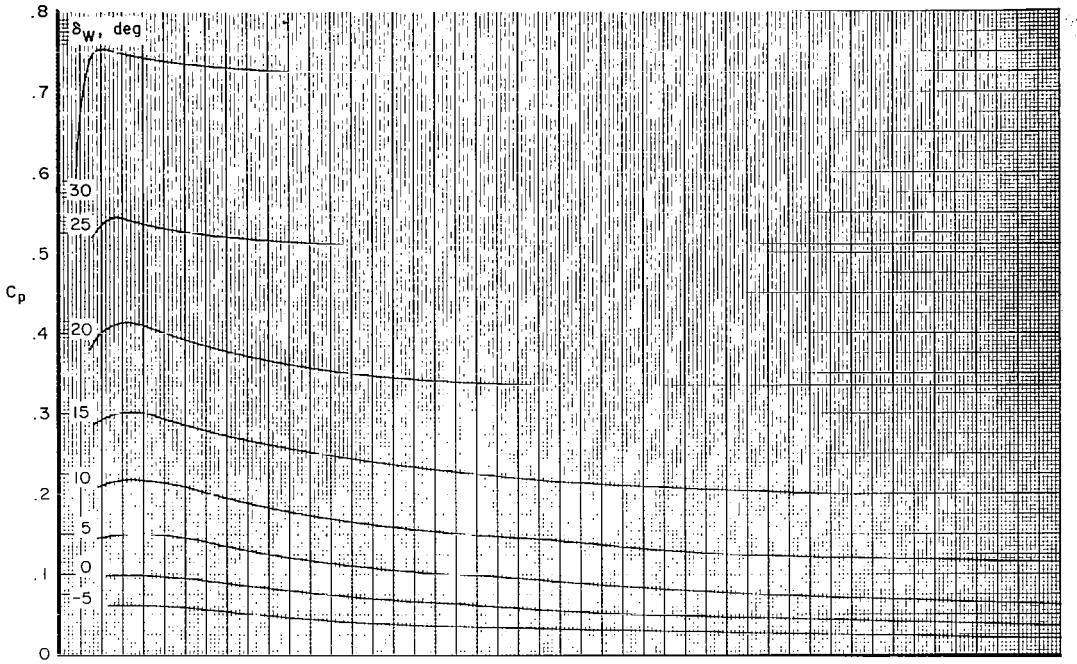


(a) $M_\infty$ 10

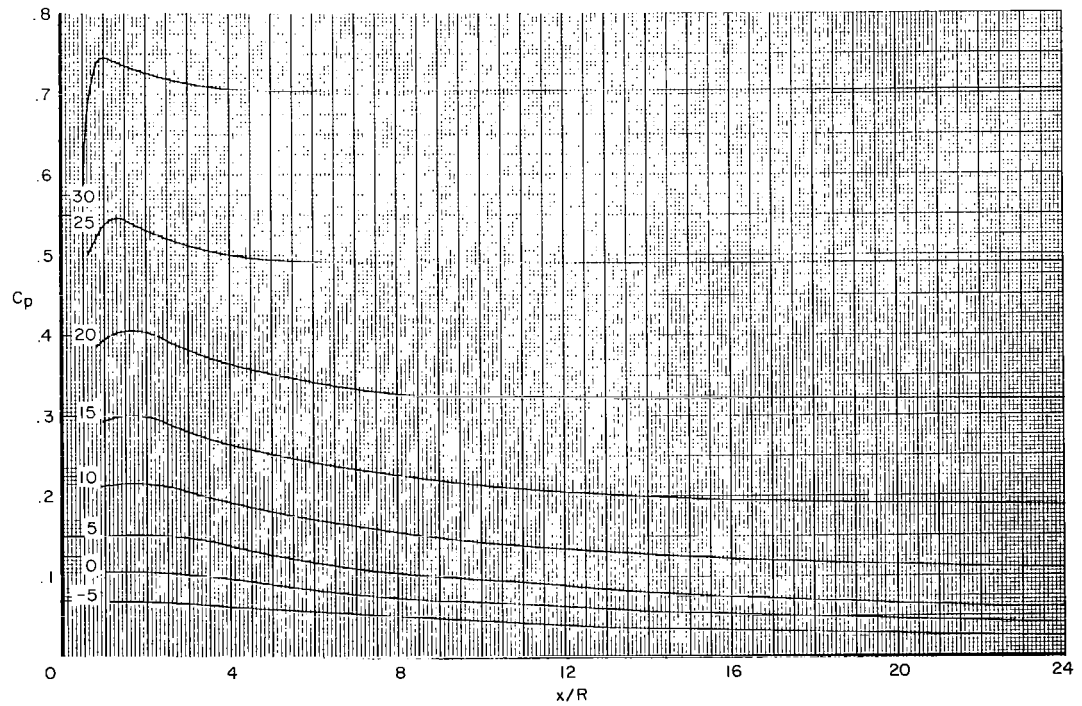


(b) $M_\infty = \infty$

Chart 2.- Pressure distribution over the blunt-wedge surface for a specific-heat ratio of 1.667.

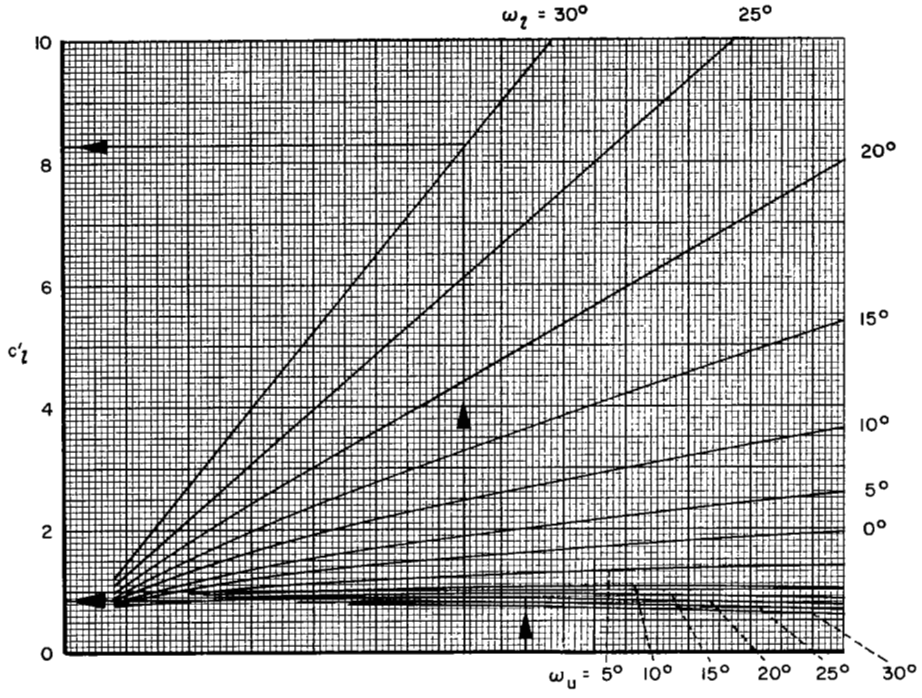


(a) $M_\infty$ = 10

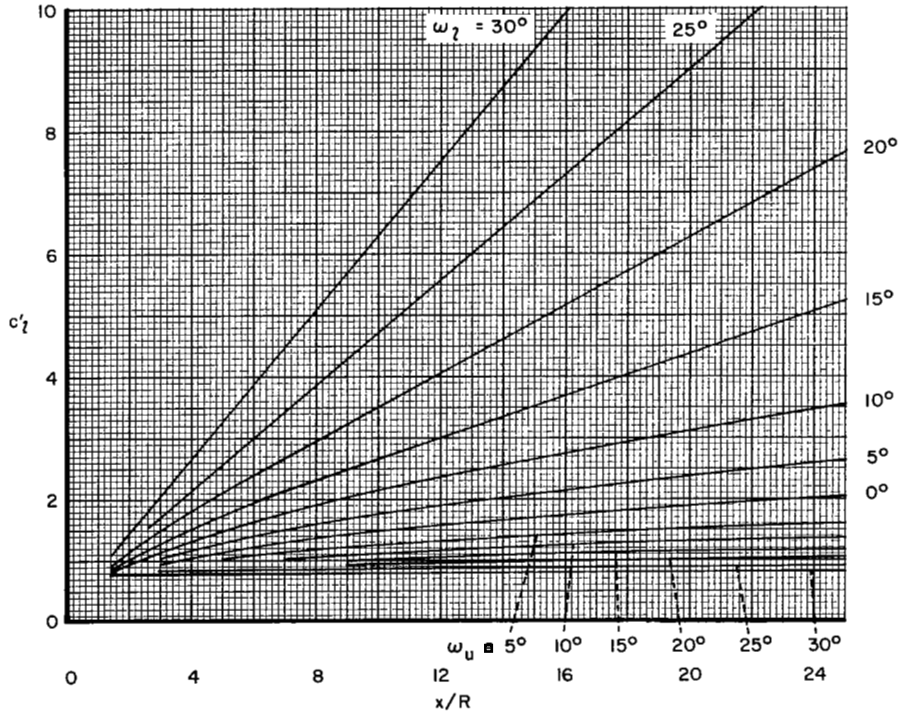


(b) $M_\infty$ = ∞

Chart 3.- Contribution of the blunt leading edge and wedge surfaces to lift coefficient for a specific-heat ratio of 1.400.

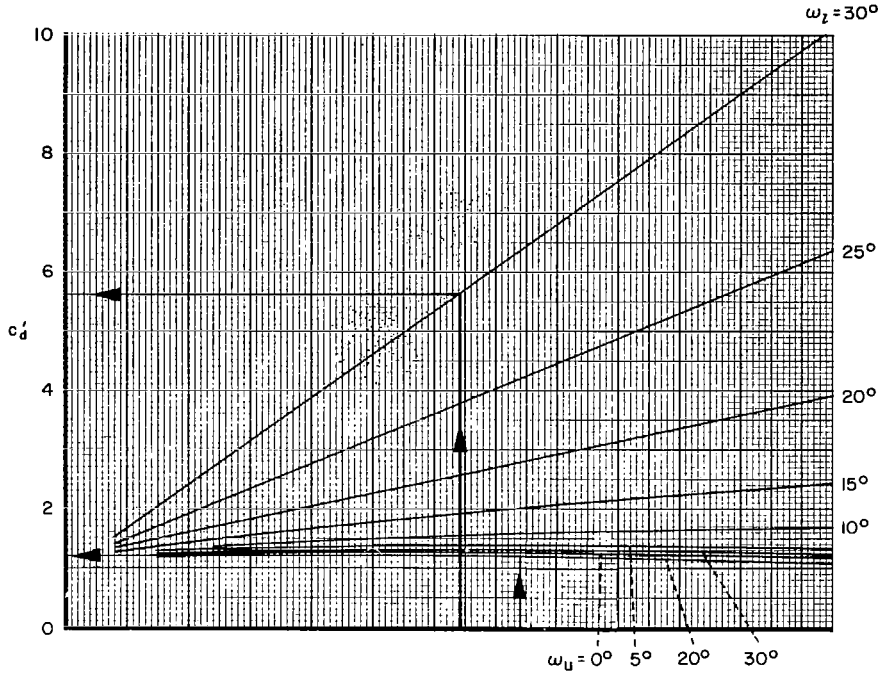


(a) $M_\infty$ - 10

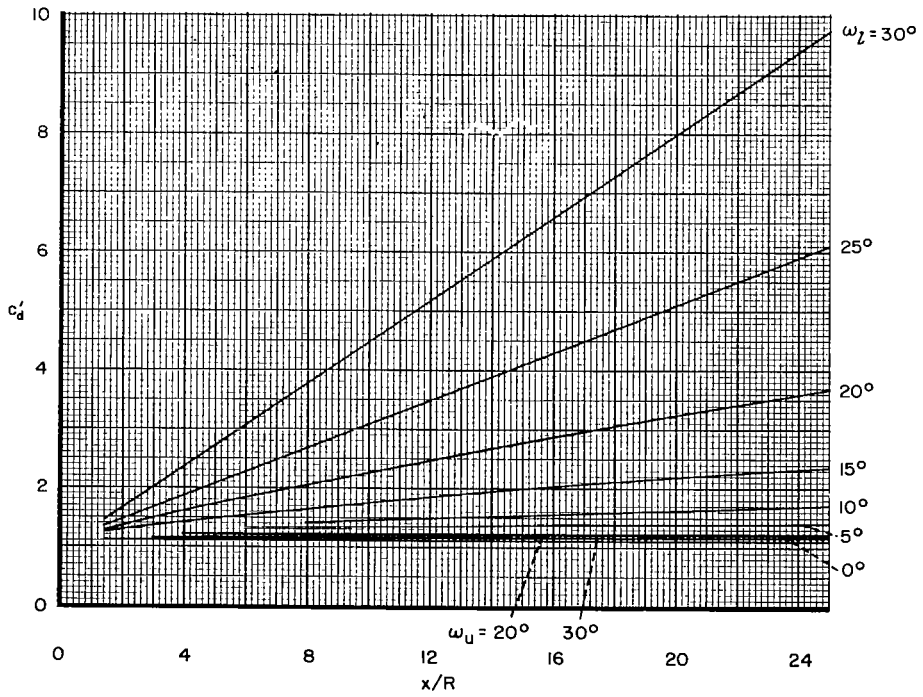


(b) $M_\infty = \infty$

Chart 4.- Contribution of the blunt leading edge and wedge surfaces to drag coefficient; $\gamma = 1.400$.

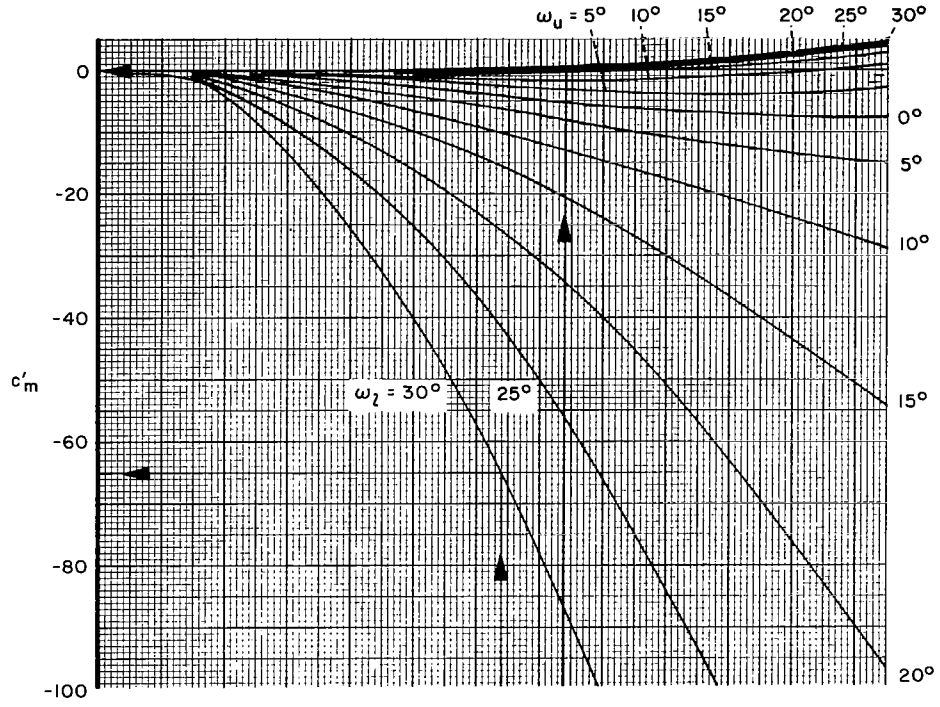


(a) $M_\infty$ = 10

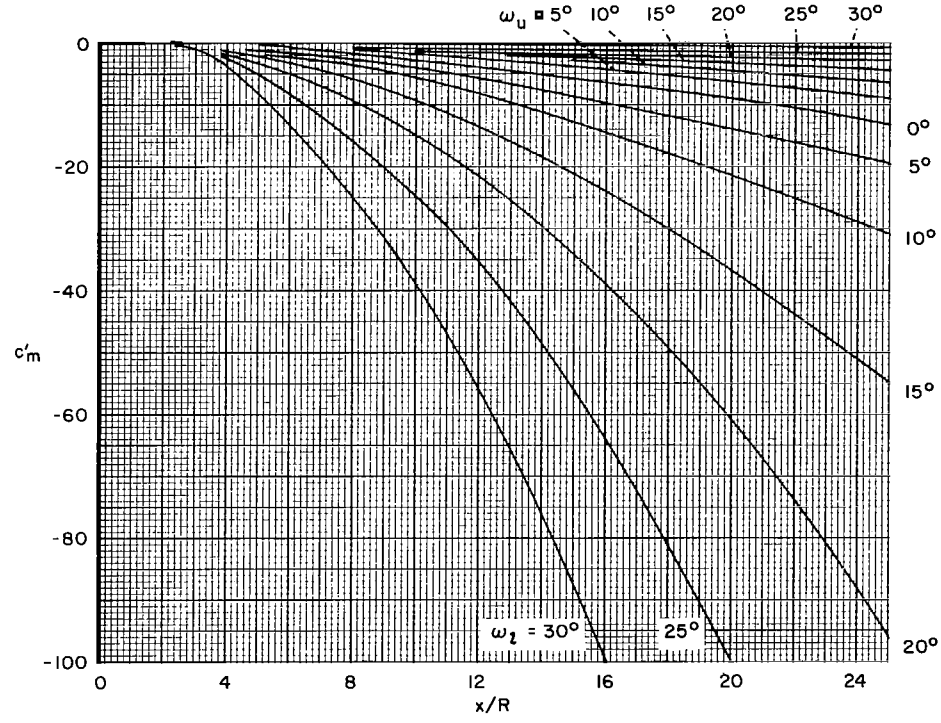


(b) $M_\infty = \infty$

Chart 5.- Contribution of the blunt leading edge and wedge surfaces to pitching-moment coefficient; $\gamma$ = 1.400.

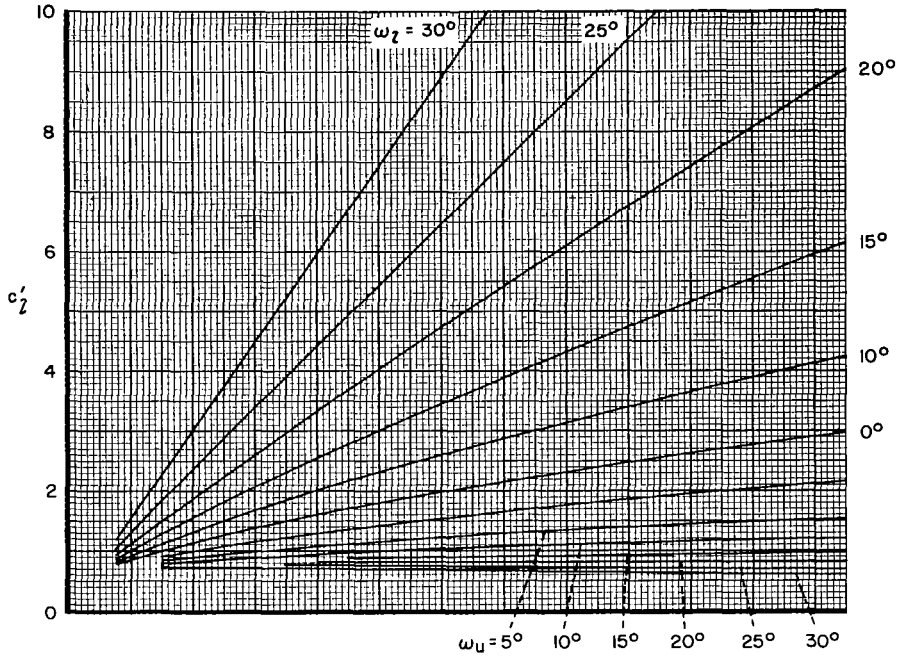


(a) $M_\infty$ = 10

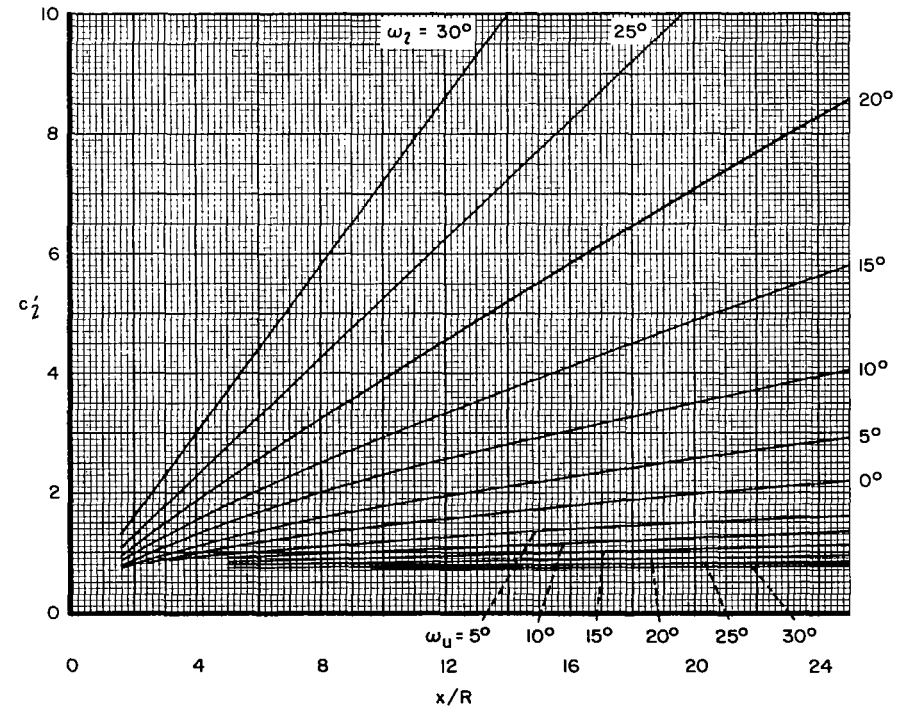


(b) $M_\infty$ = ∞

Chart 6.- Contribution of the blunt leading edge and wedge surfaces to lift coefficient for a specific-heat ratio of 1.667.

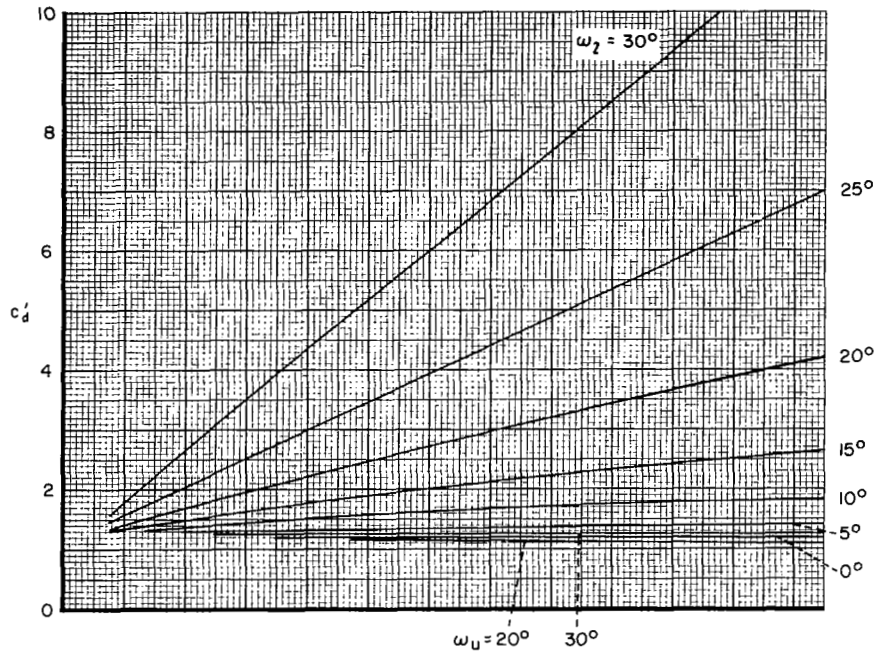


(a) $M_\infty = 10$

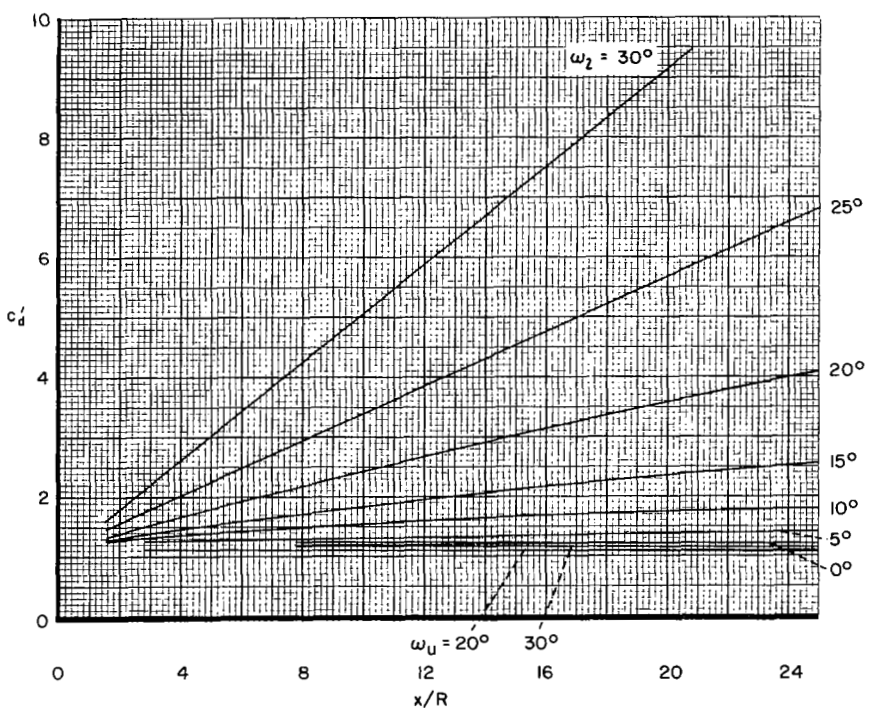


(b) $M_\infty = \infty$

Chart 7.- Contribution of the blunt leading edge and wedge surfaces to drag coefficient for a specific-heat ratio of 1.667.

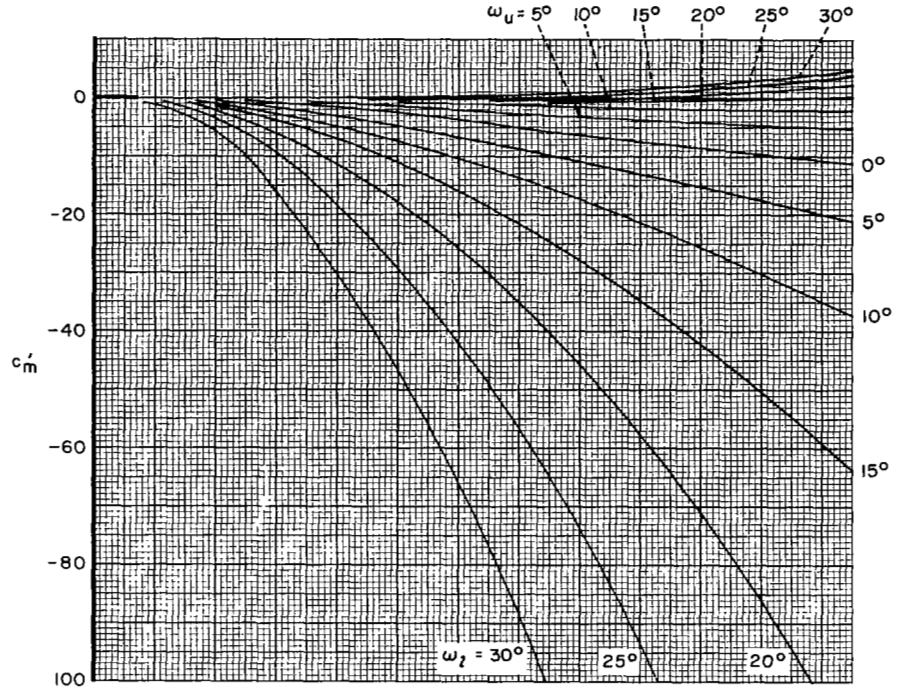


(a) $M_\infty$ = 10

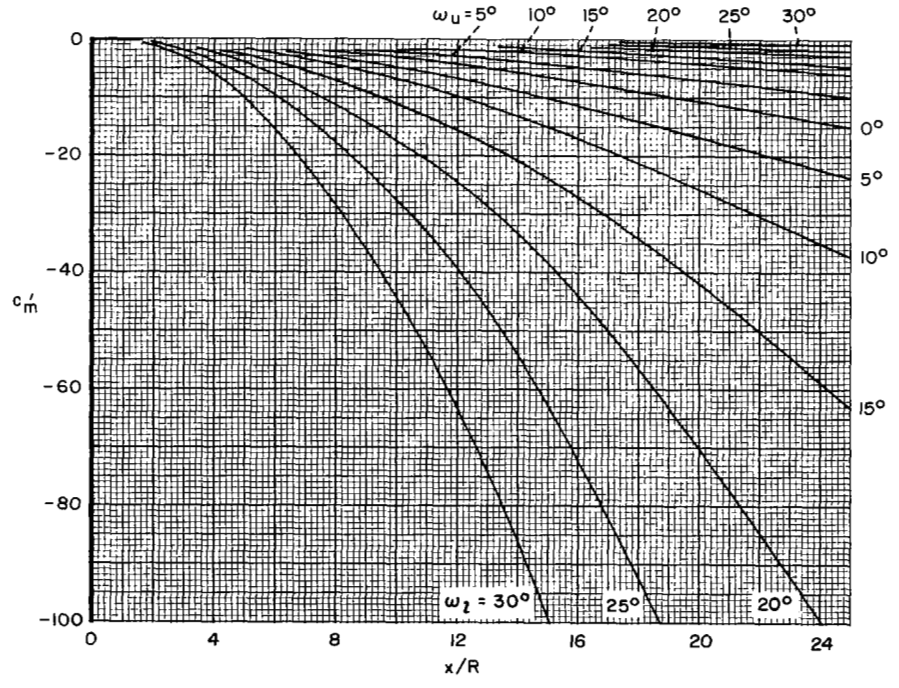


(b) $M_\infty$ = ∞

Chart 8.- Contribution of the blunt leading edge and wedge surfaces to pitching-moment coefficient for a specific-heat ratio of 1.667.

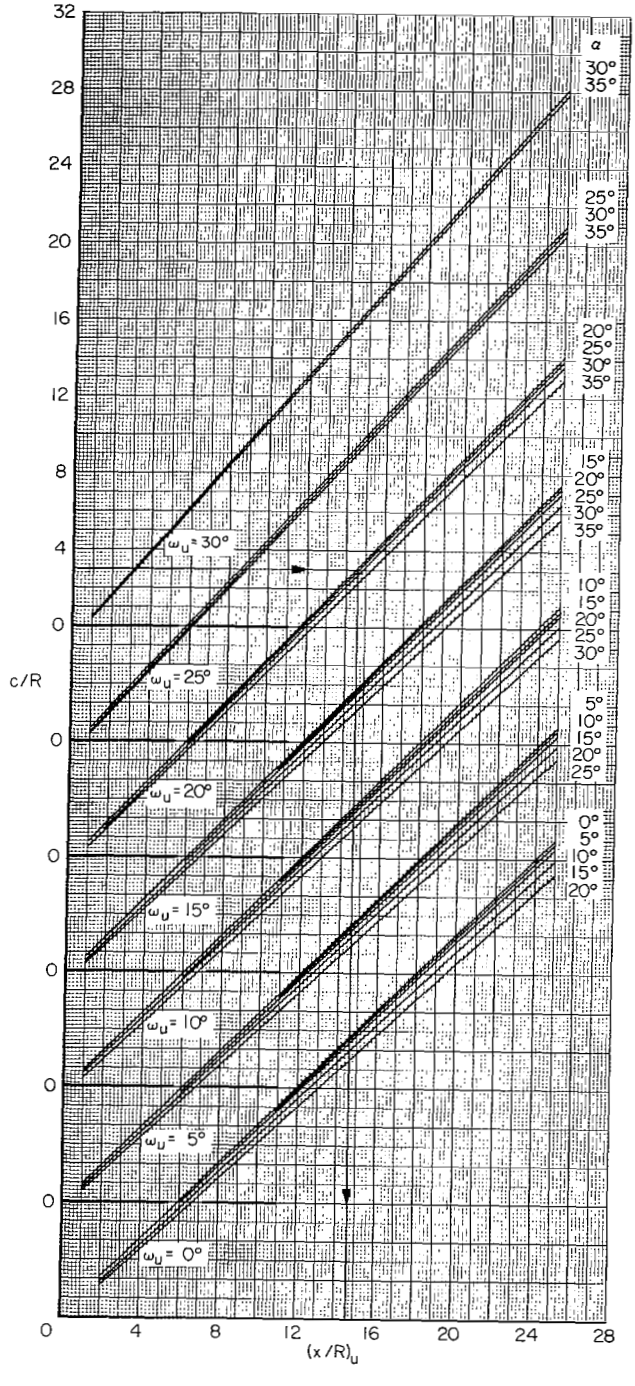


(a) Upper-surface trailing edge.

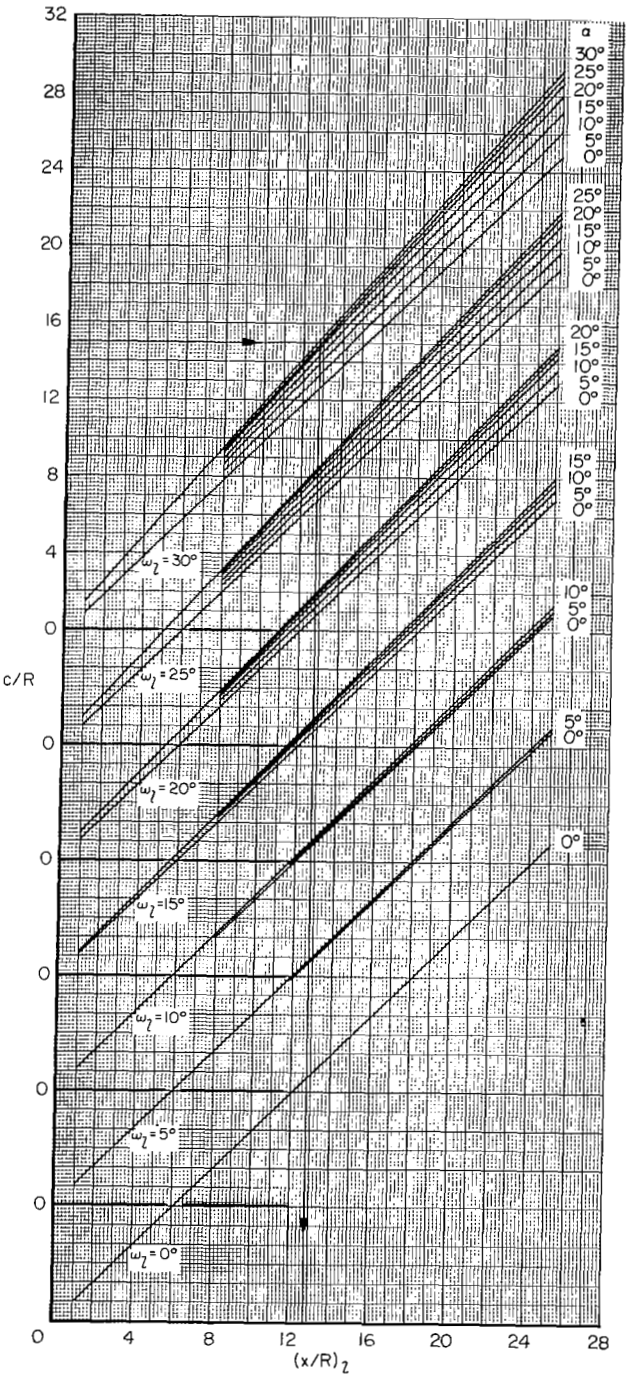


(b) Lower-surface trailing edge.

Chart 9.- Coordinate transformations of the upper- and lower-surface trailing edges.

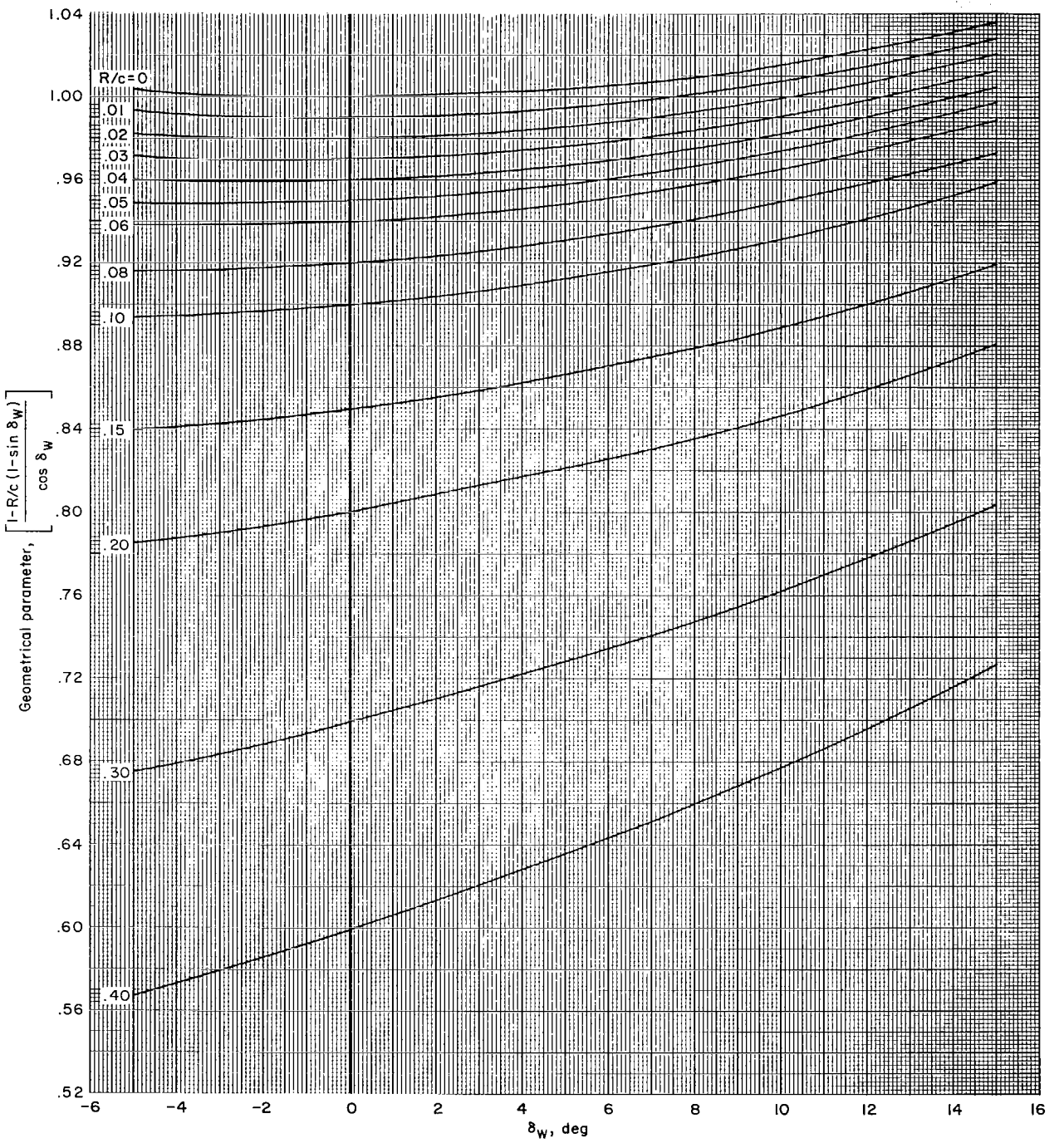


Chart 10.- A geometrical parameter of blunt wedge airfoils.